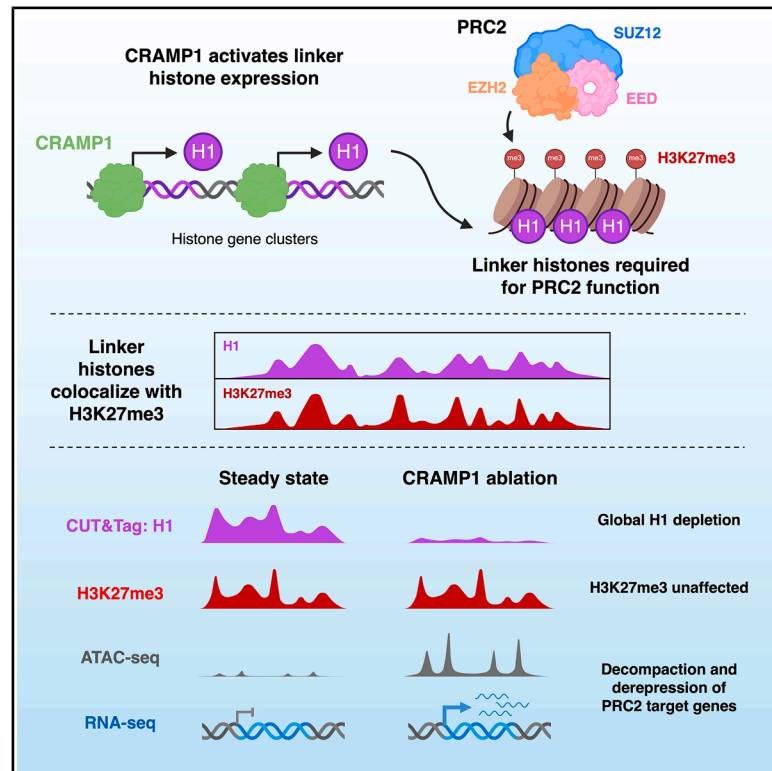


CRAMP1 drives linker histone expression to enable Polycomb repression

Graphical abstract



Authors

Rachael E. Matthews,
 Joshua Miguel C. Danac,
 Emily L. Naden, ..., Richard T. Timms,
 Julie Ahringer, Iva A. Tchasovnikarova

Correspondence

it257@cam.ac.uk

In brief

Challenging the prevailing view that H1 linker histones represent a general feature of repressed chromatin, Matthews et al. show a specific requirement for H1 in epigenetic repression by PRC2. Ablation of the H1 activator CRAMP1 results in linker histone insufficiency and derepression of PRC2 target genes.

Highlights

- A genome-wide CRISPR screen reveals *CRAMP1* is required for PRC2 repression
- CRAMP1 binds linker histone genes and drives their expression
- Linker histones are enriched at H3K27me3-marked genomic loci
- Linker histone insufficiency following CRAMP1 ablation abrogates PRC2 repression



Article

CRAMP1 drives linker histone expression to enable Polycomb repression

Rachael E. Matthews,^{1,2} Joshua Miguel C. Danac,^{1,2,8} Emily L. Naden,^{1,2,8} Laura E. Farleigh Smith,^{1,9} Sri Lestari,^{1,2} Akhila Gungi,^{1,2} Alex Appert,¹ Toby Buttress,¹ Ankit Verma,^{1,10} Oliver Sinclair,³ Faye Chong,⁴ John Suberu,⁵ Robin Antrobus,⁵ Boyan Bonev,^{4,6} Mark A. Dawson,³ Adam J. Reid,¹ Richard T. Timms,⁷ Julie Ahringer,¹ and Iva A. Tchasovnikarova^{1,2,11,*}

¹The Gurdon Institute, University of Cambridge, Tennis Court Road, Cambridge CB2 1QN, UK

²Department of Biochemistry, University of Cambridge, Tennis Court Road, Cambridge CB2 1GA, UK

³Peter MacCallum Cancer Centre, Melbourne, VIC 3000, Australia

⁴Helmholtz Pioneer Campus, Helmholtz Zentrum München, Neuherberg, Germany

⁵Department of Medicine, Cambridge Institute for Medical Research, Addenbrooke's Hospital, Hills Road, Cambridge CB2 0XY, UK

⁶Physiological Genomics, Biomedical Center, Ludwig-Maximilians-Universität München, Munich, Germany

⁷Cambridge Institute for Therapeutic Immunology and Infectious Disease, Jeffrey Cheah Biomedical Centre, Cambridge CB2 0AW, UK

⁸These authors contributed equally

⁹Present address: Division of Infection and Immunity, Cardiff University, Heath Park, Cardiff CF14 4XN, UK

¹⁰Present address: MedGenome Labs Ltd, Bengaluru 560100, Karnataka, India

¹¹Lead contact

*Correspondence: it257@cam.ac.uk

<https://doi.org/10.1016/j.molcel.2025.05.031>

SUMMARY

In contrast to the well-understood role of core histones in DNA packaging, the function of the linker histone (H1) remains enigmatic. Challenging the prevailing view that linker histones are a general feature of heterochromatin, here we show a critical requirement for H1 in Polycomb repressive complex 2 (PRC2) function. A CRISPR-Cas9 genetic screen using a fluorescent PRC2 reporter identified an essential role for the poorly characterized gene *CRAMP1* in PRC2-mediated repression. *CRAMP1* localizes to the promoters of expressed H1 genes and positively regulates their transcription. *CRAMP1* ablation simultaneously depletes all linker histones, which results in selective decompaction of H3K27me₃-marked loci and derepression of PRC2 target genes without concomitant loss of PRC2 occupancy or enzymatic activity. Strikingly, we find that linker histones preferentially localize to genomic loci marked by H3K27me₃ across diverse cell types and organisms. Altogether, these data demonstrate a prominent role for linker histones in epigenetic repression by PRC2.

INTRODUCTION

The histone proteins allow for meters of eukaryotic DNA to be packaged into a ~10 μm nucleus while ensuring that the DNA can still be accessed during transcription, replication, and repair. The indispensable role of the four core histones (H2A, H2B, H3, and H4) in nucleosomal DNA packaging is well understood, but defining the function of the linker histone (H1) represents a long-standing challenge. Unlike the core histones, H1 is dispensable for the chromatinization of DNA *in vitro*: nucleosome arrays still assemble into a “beads-on-a-string” conformation in the absence of linker histones.¹ Instead, as a result of its ability to bind to the nucleosomal DNA entry/exit site and condense nucleosome arrays to form the so-called “30 nm fiber,^{2,3}” histone H1 has long been postulated to act as a general component of heterochromatin.⁴ However, *in vivo* depletion of histone H1 in both unicellular and multicellular organisms results in the dere-

pression of specific subsets of genes,^{5–8} which is difficult to reconcile with the notion of linker histones acting broadly as heterochromatic factors with little specificity in their genomic distribution.^{9–18}

The existence of multiple H1 subtypes and variants complicates the study of linker histones *in vivo*. In mice and in humans there are eleven genes encoding H1 subtypes: seven are somatic (H1.1–H1.5, plus H1.0 and H1X), three are testis-specific (H1t, H1T2, and HILS1), and one is restricted to oocytes (H1oo).^{4,19} Among the somatic H1 subtypes, H1.1 through H1.5 are considered “replication-dependent” as their expression increases during S-phase, whereas the H1.0 and H1X variants are termed “replication-independent” as they are expressed throughout the cell cycle. Individual or pairwise knockout (KO) of H1 genes (H1.0, H1.2, H1.3, or H1.4) does not noticeably perturb murine development,²⁰ but examination of germinal center B cells derived from H1.2/H1.4 double KO



mice identified multiple defects in chromatin compartmentalization and transcriptional repression.²¹ Discordant phenotypes have also been described in triple KO cells lacking histones H1.2, H1.3, and H1.4, with few transcriptional changes noted in mouse embryonic stem cells²² but derepression of thousands of genes observed in CD8⁺ T cells.^{23,24} Overall, mechanistic progress is hampered by an inability to acutely deplete cells of all linker histones simultaneously.

Here, we identify CRAMP1 as a critical activator of linker histone gene expression. CRAMP1 knockdown results in simultaneous depletion of all H1 subtypes and variants, providing a unique tool to interrogate the functional role of linker histones in human cells. We find that linker histones are critically required for repression by Polycomb repressive complex 2 (PRC2). H1 predominantly localizes to chromatin marked by H3K27me3, and H1 depletion achieved via CRAMP1 knockdown results in derepression of PRC2 target genes through chromatin decompaction without affecting PRC2 recruitment or enzymatic activity.

RESULTS

A genome-wide CRISPR-Cas9 genetic screen identifies an essential role for CRAMP1 and histone H1.4 in PRC2-mediated silencing

Polycomb-group (PcG) proteins are critical chromatin regulators that maintain cell fate through the repression of lineage-inappropriate genes.²⁵ Biochemical characterization of PcG proteins in mammals has identified multiple Polycomb repressive complexes—prominently PRC1 and PRC2—both of which encompass multiple subcomplexes (Figures S1A and S1B). PRC1 complexes are thought to exert their function through monoubiquitylation of histone H2A at Lys119 (H2AK119ub1)^{26,27} and chromatin compaction,^{28,29} while PRC2 complexes are thought to instill repression by trimethylating histone H3 at Lys27 (H3K27me3).^{30–33}

We previously exploited transgene reporters across chromatin environments (TRACE), a high-throughput approach that identifies phenotypic reporters for epigenetic factors, to generate a fluorescent reporter cell line responsive to loss of the PRC2 subunit SUZ12.³⁴ Further characterization of this KBM-7 reporter clone revealed that disruption of any of the three core PRC2 subunits, but not components of PRC1 complexes, resulted in reporter derepression (Figures 1A, 1B, S1A, and S1C). To identify additional factors required for PRC2 function, we exploited our reporter clone to perform a genome-wide CRISPR-Cas9 genetic screen. We reasoned that mutant cells lacking genes required for PRC2 function would exhibit derepression of the reporter, generating GFP^{bright} cells that could be isolated by fluorescence-activated cell sorting (FACS) (Figure 1C). The top hits from the screen were the histone H1 subtype *HIST1H1E* (encoding histone H1.4), the PRC2.1 accessory factor *MTF2* (also known as Polycomb-like protein 2 or PCL2), and *CRAMP1*, a poorly characterized gene of unknown function (Figure 1C; Table S1). We validated an essential requirement for these three genes in reporter repression through individual CRISPR-Cas9-mediated gene disruption experiments (Figure 1D). By contrast, disruption of the Polycomb-like proteins PHF1 and PHF19 did not result in GFP dere-

pression (Figures S1B and S1D), suggesting that the reporter line responds specifically to loss of PRC2.1 complexes harboring MTF2. Moreover, the functional association between CRAMP1, linker histones, and PRC2 subunits is supported by their co-essential relationships across hundreds of human cell lines profiled by the Dependency Map (DepMap) project³⁵ (Figure 1E).

CRAMP1 binds transcriptionally active histone genes

Subcellular fractionation experiments indicated that CRAMP1 is a nuclear protein that can localize to chromatin (Figure 2A), and so we performed cleavage under targets and release under nuclease (CUT&RUN) analysis in K562 cells to assess its genome-wide occupancy. Strikingly, we found that the majority of CRAMP1 peaks (68%) were located at the promoters of histone genes (Figures 2B, 2C, and S2A; Table S2). Supporting the specificity of the commercial antibody against CRAMP1, exogenous CRAMP1 expressed with a V5 epitope tag displayed a near-identical distribution (Figures 2B and 2C). CRAMP1 bound the promoters of both replication-dependent and replication-independent histone genes encompassing all five families (H1, H2A, H2B, H3, and H4; $n = 56$ out of 90) (Figures 2C, S2B, and S2C). Notably, histone genes that were not bound by CRAMP1 were not expressed (Figures 2C–2E and S2D); thus, CRAMP1 occupancy is almost entirely restricted to transcriptionally active histone genes.

CRAMP1 is required for full expression of linker histone genes

The specificity of CRAMP1 for expressed histone genes suggested that CRAMP1 might be required for histone gene expression, and so we performed RNA sequencing (RNA-seq) in K562 cells following short hairpin RNA (shRNA)-mediated depletion of CRAMP1 (Figure S2E). Despite the localization of CRAMP1 to all five families of histone genes, only linker histone expression was affected by CRAMP1 loss: each of the five H1 genes expressed in K562 cells (H1.2, H1.3, H1.4, H1.5, and H1X) were downregulated ~2-fold (Figures 3A, 3B, and S2F). We were readily able to confirm the requirement for CRAMP1 for histone H1 expression by both immunoblot (Figure 3C) and quantitative reverse transcription PCR (RT-qPCR) (Figure 3D) following CRISPR-Cas9-mediated gene disruption of CRAMP1 (Figure S2G). Thus, although CRAMP1 binds to the promoters of genes encoding both core histones and linker histones, we conclude that this previously uncharacterized protein is required to drive the full expression of H1 genes.

Exogenous expression of linker histones relieves the requirement for CRAMP1

As histone H1.4 also emerged from our genetic screen (Figure 1C), a functional role for CRAMP1 in facilitating H1 expression was intriguing. Supporting the notion that the requirement for CRAMP1 could be explained by its role in driving linker histone expression, we found that repression of our fluorescent PRC2 reporter in CRAMP1 KO cells could not only be restored upon exogenous expression of CRAMP1, but also partially by exogenous expression of histone H1.4 (Figures 3E, S2H, and S2I). This effect was not restricted to H1.4, however, as all the linker histone subtypes and variants that we examined

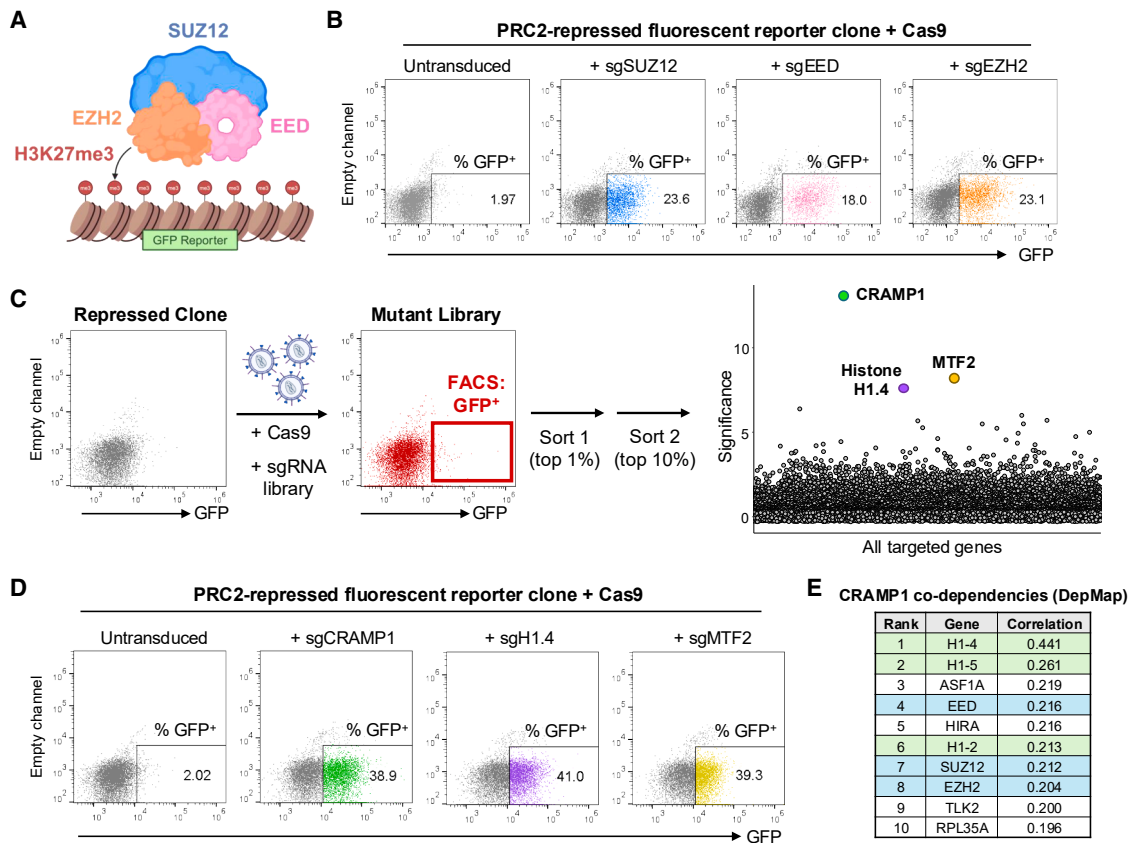


Figure 1. A genome-wide CRISPR-Cas9 genetic screen identifies an essential requirement for CRAMP1 and histone H1.4 in PRC2-mediated reporter repression

(A) Schematic representation of GFP reporter repression by the PRC2 complex.

(B) The GFP reporter is derepressed upon CRISPR-Cas9-mediated gene disruption of any of the three core PRC2 subunits, as assayed by flow cytometry.

(C) A genome-wide CRISPR-Cas9 screen to identify factors required for PRC2 function. Following Cas9 expression in KBM-7 cells harboring the PRC2-sensitive GFP reporter, genome-wide mutagenesis was carried out with the Sabatin/Lander single guide RNA (sgRNA) library,³⁶ and GFP⁺ cells isolated through two sequential rounds of FACS. “Significance” on the y axis represents the negative log of the “pos|score” metric reported by Model-based Analysis of Genome-wide CRISPR-Cas9 Knockout (MAGeCK).³⁷

(D) Validation of the screen hits through individual CRISPR-Cas9-mediated gene disruption of *CRAMP1*, *H1.4*, and *MTF2*. GFP reporter derepression was measured by flow cytometry.

(E) The functional requirement for CRAMP1 and linker histones in PRC2 function is conserved across hundreds of human cell lines. Analysis of the top 10 CRAMP1 co-dependencies in DepMap revealed three linker histones (green) and all core members of the PRC2 complex (blue). Correlation values represent Pearson correlation as reported by DepMap.

See also [Figure S1](#) and [Table S1](#).

were able to restore reporter repression, albeit to varying extents ([Figure S2H](#)). We also interrogated four endogenous target genes, where we found that exogenous expression of H1.4 counteracted the derepression resulting from CRAMP1 depletion ([Figures S2J](#) and [S2K](#)). Therefore, the essential requirement for CRAMP1 in PRC2-mediated reporter repression can be explained by its role as an activator of linker histone expression.

CRAMP1 is a member of the histone gene regulatory machinery

Next we considered the mechanism through which CRAMP1 might regulate the expression of linker histone genes. Three key regulators of histone gene expression have been identified: nuclear protein, ataxia-telangiectasia locus (NPAT), GON-4-like protein (GON4L), also known as YARP, and FLICE-associated

huge protein (FLASH).^{38–40} FLASH is required for the generation of mature histone mRNAs following the 3' end cleavage of histone pre-mRNAs.⁴¹ The role of GON4L remains poorly understood, though studies in mice and *Drosophila* have suggested it acts as a transcriptional repressor.^{42,43} Both FLASH and GON4L utilize Swi3, Ada2, N-CoR, and TFIIB (SANT) domains to bind the C terminus of NPAT, which is considered the key transcriptional activator of histone gene expression.^{38,44,45} To assess whether CRAMP1 might act in concert with these known regulators, we sought to identify CRAMP1 binding partners. Immunoprecipitation of V5-tagged CRAMP1 from nuclear lysates followed by mass spectrometry identified GON4L as a candidate interactor at high confidence ([Figure 3F](#); [Table S3](#)). Furthermore, large-scale interactomics⁴⁶ has identified both GON4L and NPAT as CRAMP1 binding partners, and we were

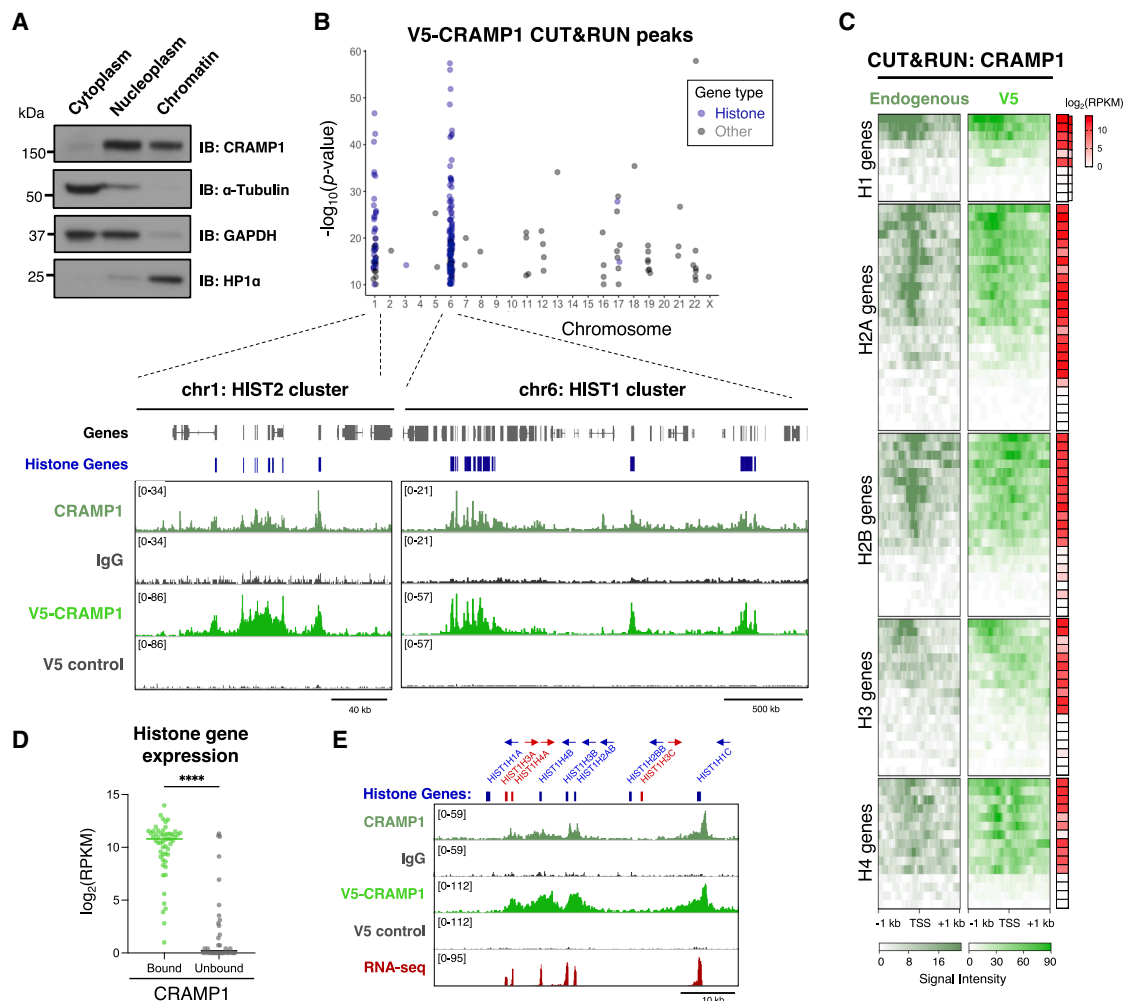


Figure 2. CRAMP1 binds to the promoters of histone genes

(A) Subcellular fractionation of K562 cells assessed by immunoblot. HP1 α , GAPDH, and α -tubulin were used to validate the fractionation. (B–E) CRAMP1 localizes to the promoters of transcriptionally active histone genes. (B) CUT&RUN analysis of V5-tagged CRAMP1 in K562 cells identified 230 high-confidence peaks, the majority of which were located within the HIST1 and HIST2 histone gene clusters. (C) CRAMP1 occupies the promoters of expressed histone genes from all five families. The heatmaps represent occupancy of either endogenous CRAMP1 (dark green, left) or V5-CRAMP1 (light green, right) across all histone gene as measured by CUT&RUN. Genes are grouped by histone family and ordered by CRAMP1 signal intensity. Gene expression, as measured by RNA-seq, is displayed as a heatmap in red. (D) Histone genes bound by CRAMP1 (green) are more highly expressed than those not bound (gray). (**** $p < 0.0001$; two-tailed Mann-Whitney test). Example histone genes are shown in (E). See also [Figure S2](#) and [Table S2](#).

able to confirm these interactions by immunoprecipitation followed by immunoblot ([Figure 3G](#)). Thus, these data suggest that CRAMP1 physically associates with known regulators of histone gene expression.

The only annotated feature of CRAMP1 is an N-terminal SANT domain. Structural bioinformatic analysis suggests an ordered domain (“DomII”) immediately downstream of the SANT domain, as well as a ubiquitin-like (UBL) domain bifurcated by a 214-amino acid disordered region ([Figure 3H](#)). To assess which of these domains are essential for CRAMP1 function, we performed genetic complementation experiments to test the ability of CRAMP1 deletion mutants to restore repression of our fluorescent PRC2 reporter clone following CRAMP1 KO. While exoge-

nous expression of full-length CRAMP1 resulted in re-repression of the GFP reporter, deletion of any of the three structured domains abolished CRAMP1 activity ([Figures 3H, 3I, and S3A](#)). Furthermore, by CUT&RUN, we found that each deletion mutant severely abrogated occupancy at histone gene promoters, suggesting that all three domains contribute to CRAMP1 localization ([Figures S3B and S3C](#)).

As both GON4L and FLASH bind the C terminus of NPAT through their SANT domains,⁴⁷ we wondered whether the SANT domain of CRAMP1 might act in a similar manner. Indeed, AlphaFold 3⁴⁸ proposes that the CRAMP1 SANT domain engages the C-terminal α helix of NPAT in an analogous manner to that of GON4L and FLASH ([Figures 3J and S3D](#)). In support of this model,

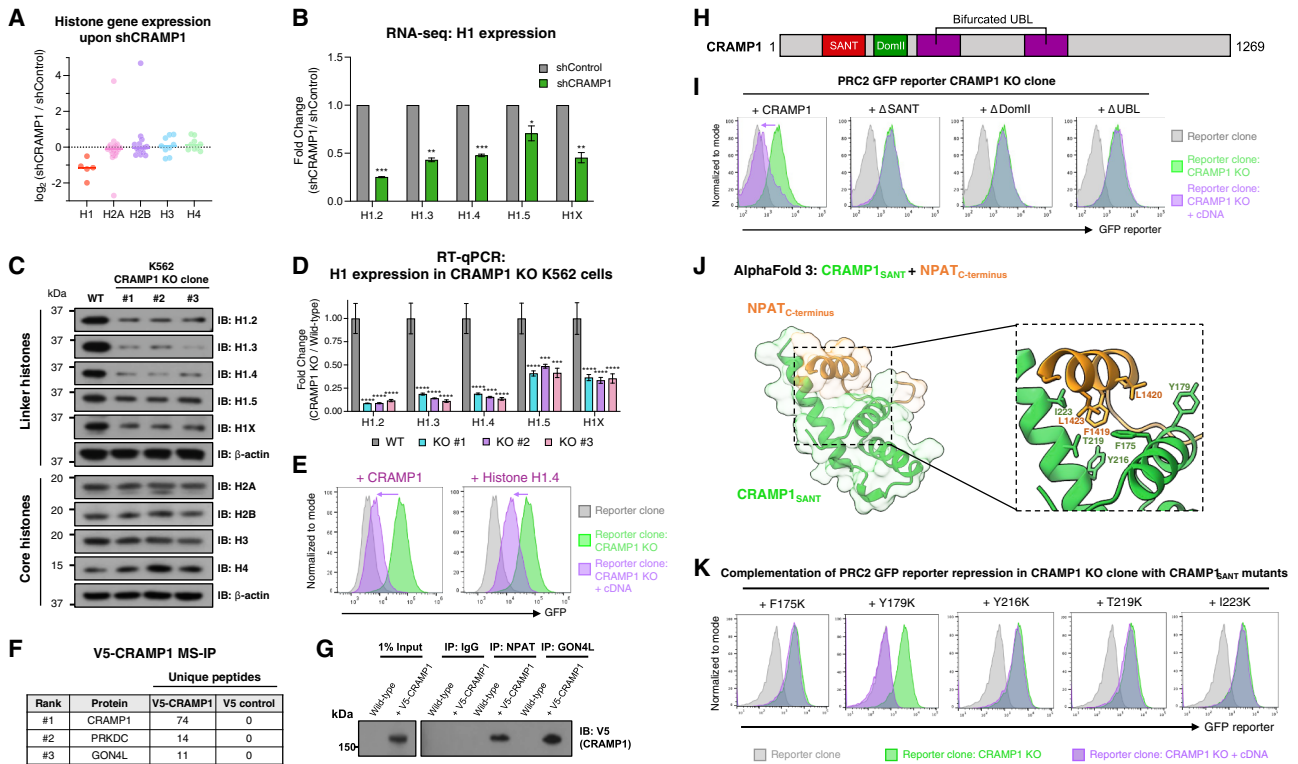


Figure 3. CRAMP1 regulates the expression of linker histone genes

(A–D) Loss of CRAMP1 reduces linker histone expression. (A) Histone gene expression upon CRAMP1 knockdown as measured by RNA-seq. Only expressed histone genes are shown (** $p < 0.01$; Wilcoxon signed rank test against 0). (B) Downregulation of all expressed linker histones upon CRAMP1 depletion. Plots show mean \pm SD of three technical replicates (* $p < 0.05$, ** $p < 0.01$, *** $p < 0.001$ versus shControl, unpaired one-sample t test with Holm-Sidak correction for multiple comparisons). (C) CRAMP1 KO clones express reduced levels of linker histone proteins (top) but not core histone proteins (bottom), as measured by immunoblot. (D) Reduced levels of linker histone transcripts in CRAMP1 KO cells as measured by RT-qPCR. Plots show mean \pm SD of three technical replicates (** $p < 0.001$, *** $p < 0.0001$ versus wild-type [WT], one-way ANOVA with Dunnett's test for multiple comparisons). (E) Exogenous expression of histone H1.4 is sufficient to restore GFP reporter repression in the absence of CRAMP1. The indicated cDNAs were introduced into the CRAMP1 KO KBM-7 reporter clone by lentiviral transduction, and GFP fluorescence was assessed by flow cytometry. (F and G) CRAMP1 interacts with known regulators of histone gene expression. (F) Immunoprecipitation of V5-CRAMP1 followed by mass spectrometry identified GON4L as a CRAMP1 binding partner; V5-CRAMP1 immunoprecipitation followed by immunoblot validated GON4L and NPAT as CRAMP1 interactors (G). (H and I) The ordered domains of CRAMP1 are all required for its function. (H) Domain architecture of CRAMP1. (I) Genetic complementation of CRAMP1 KO cells. The indicated CRAMP1 mutants were introduced into CRAMP1 KO KBM-7 reporter clone by lentiviral transduction, and GFP fluorescence was assessed by flow cytometry. (J and K) The SANT domain of CRAMP1 mediates the interaction with NPAT. (J) AlphaFold 3 structural model proposing that the SANT domain of CRAMP1 engages the C terminus of NPAT. (K) Validation of the model through mutation of putative interface residues. The indicated CRAMP1 mutants were introduced into CRAMP1 KO KBM-7 reporter clone by lentiviral transduction, and GFP fluorescence was assessed by flow cytometry. See also [Figures S2](#) and [S3](#) and [Table S3](#).

mutation of residues lying on the putative CRAMP1-NPAT interface rendered CRAMP1 unable to rescue reporter repression in CRAMP1 KO cells ([Figures 3K](#), [S3E](#), and [S3F](#)). In addition, AlphaFold 3 also proposes with high confidence an interaction between the UBL domain of CRAMP1 and the paired amphipathic helix (PAH) domains of GON4L ([Figure S3G](#)). Thus, we conclude that CRAMP1 is a hitherto unrecognized component of the histone gene regulation machinery.

Linker histones localize to genomic sites marked by H3K27me3

The results from our unbiased genetic screen, together with the requirement for CRAMP1 to drive linker histone expression, sug-

gested a critical role for histone H1 in PRC2-mediated repression. To further examine the relationship between linker histones and PRC2, we sought to define the genomic distribution of H1 subtypes expressed in K562 cells ([Figure S2F](#)). Previous chromatin immunoprecipitation sequencing (ChIP-seq) studies have suggested that linker histones assume a broad genomic distribution and exhibit little specificity for particular chromatin environments^{9–18,24,49} ([Figure S4A](#)). By contrast, using cleavage under targets and tagmentation (CUT&Tag),⁵⁰ a technique that does not compromise the integrity of linker DNA, we observed a distinct pattern of H1 occupancy that was consistent among all four H1 subtypes ([Figure 4A](#)). Although it has been previously suggested that H1 subtypes display some differences in their genomic

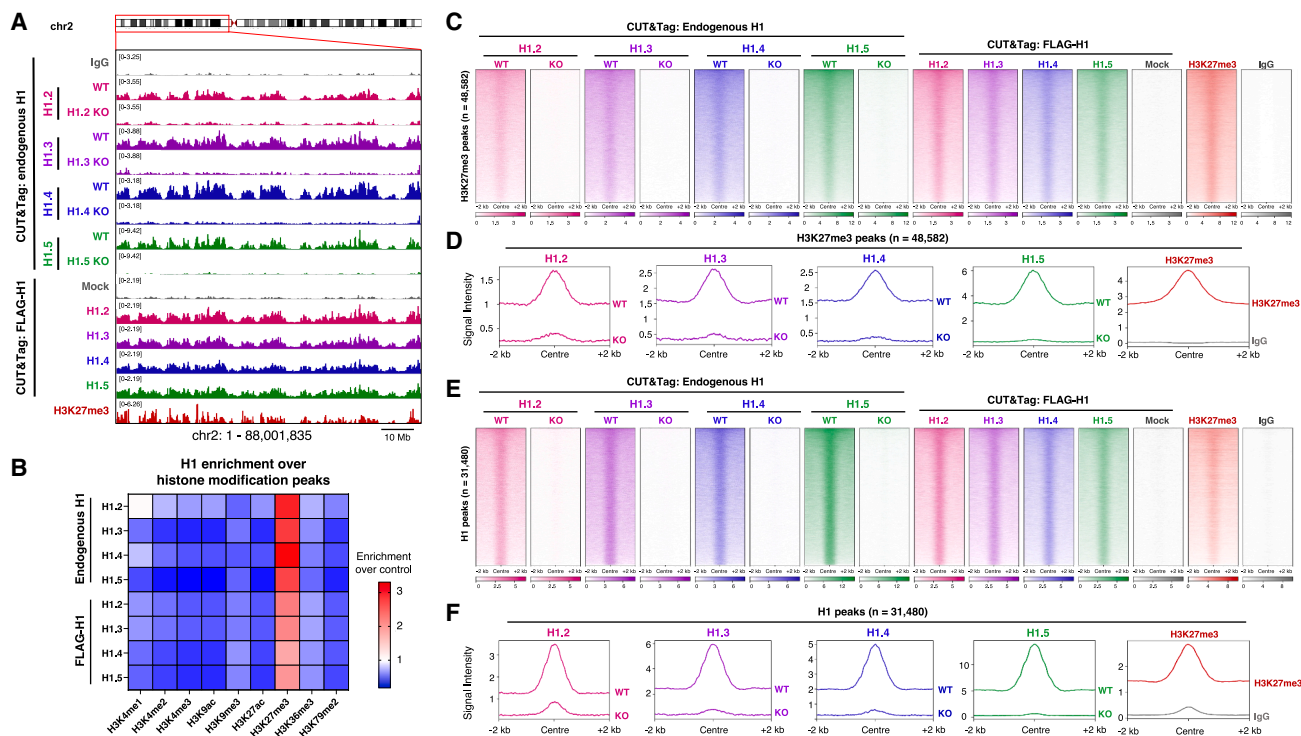


Figure 4. Linker histones localize to genomic regions marked by H3K27me3

(A) Linker histone occupancy as measured by CUT&Tag in K562 cells. The genomic distribution of linker histones is consistent across endogenous (top) and FLAG-tagged (bottom) histone subtypes and closely mirrors that of the H3K27me3 modification. See also Figure S4F.

(B–F) Linker histones colocalize with H3K27me3. (B) Heatmap depicting the enrichment of endogenous H1 (top) and FLAG-H1 (bottom) CUT&Tag signal across histone modification peaks profiled by the ENCODE project. Enrichment over control values represents H1 CUT&Tag signal over immunoglobulin G (IgG), where values >1 (red) indicate enrichment and values <1 (blue) indicate depletion. (C) Tornado plots showing that linker histones localize to the overwhelming majority of H3K27me3-marked loci. Average signal intensity across all H3K27me3 peaks is depicted in (D); H1 KO cell lines are shown as negative controls. (E) Tornado plots showing that H3K27me3 decorates the overwhelming majority of H1 peaks. Average signal intensity across all H1 peaks is depicted in (F), and H1 KO cell lines are shown as negative controls.

See also Figures S4 and S5 and Tables S2, S4, S5, and S7.

localization,^{9,13,14,51,52} we found that the four replication-dependent H1 subtypes in K562 cells exhibited near-identical localization (Figure S4B). This could not be explained by cross-reactivity of the H1 antibodies, as we confirmed antibody specificity using H1 KO clones (Figures 4A, 4C–4F, and S4C). In addition, we observed highly concordant results upon exogenous expression of H1 constructs harboring a FLAG epitope tag (Figures 4A, 4C–4F, S4B, and S4D–S4F).

To establish the chromatin features associated with H1 occupancy, we quantified the degree of overlap between H1 and a panel of histone modifications previously profiled in K562 cells through the ENCODE project.⁵³ Strikingly, this analysis revealed a positive correlation between histone H1 occupancy and a single histone modification, H3K27me3 (Figure 4B). H3K27me3-marked genomic loci were occupied by all H1 subtypes (Figures 4C–4F and S4G). We observed concordant localization between linker histones and H3K27me3 across multiple human cell types (Figures S5A–S5C; Tables S4, S5, and S6). Moreover, histone H1 overlaps with H3K27me3 domains in primary murine CD8⁺ T cells²⁴ as measured by CUT&Tag (Figure S5D), as does the H1 variant HIS-24 in *Caenorhabditis elegans* L3 larvae as

measured by ChIP-seq (Figures S5E–S5G; Table S7). We also profiled histone H1.4 occupancy in CRAMP1 KO cells, which revealed global depletion from all H3K27me3-marked genomic loci (Figures S5H–S5J).

Although linker histones have classically been considered a general feature of heterochromatin,¹⁹ we observed little overlap between H1 subtypes and H3K9me3 (Figures 4B and 5A–5D), a histone modification classically associated with constitutive heterochromatin. This could not be explained by an inability of the Tn5 transposase to access genomic loci marked by H3K9me3, as, in agreement with ChIP-seq data,⁵³ H3K9me3 profiled by CUT&Tag was enriched at Krüppel-associated box (KRAB) zinc-finger clusters, long interspersed nuclear element-1 (LINE-1) repeats, and endogenous retrovirus (ERV) elements (Figure 5E). We also tested the requirement for linker histones in H3K9me3-dependent silencing using a dual-color functional reporter assay (Figure 5F), wherein we found that linker histone insufficiency resulting from CRAMP1 depletion did not affect the H3K9me3-dependent silencing of a LINE-1 reporter by the Human Silencing Hub (HUSH) complex⁵⁴ (Figure 5G). Altogether, these data suggest that linker

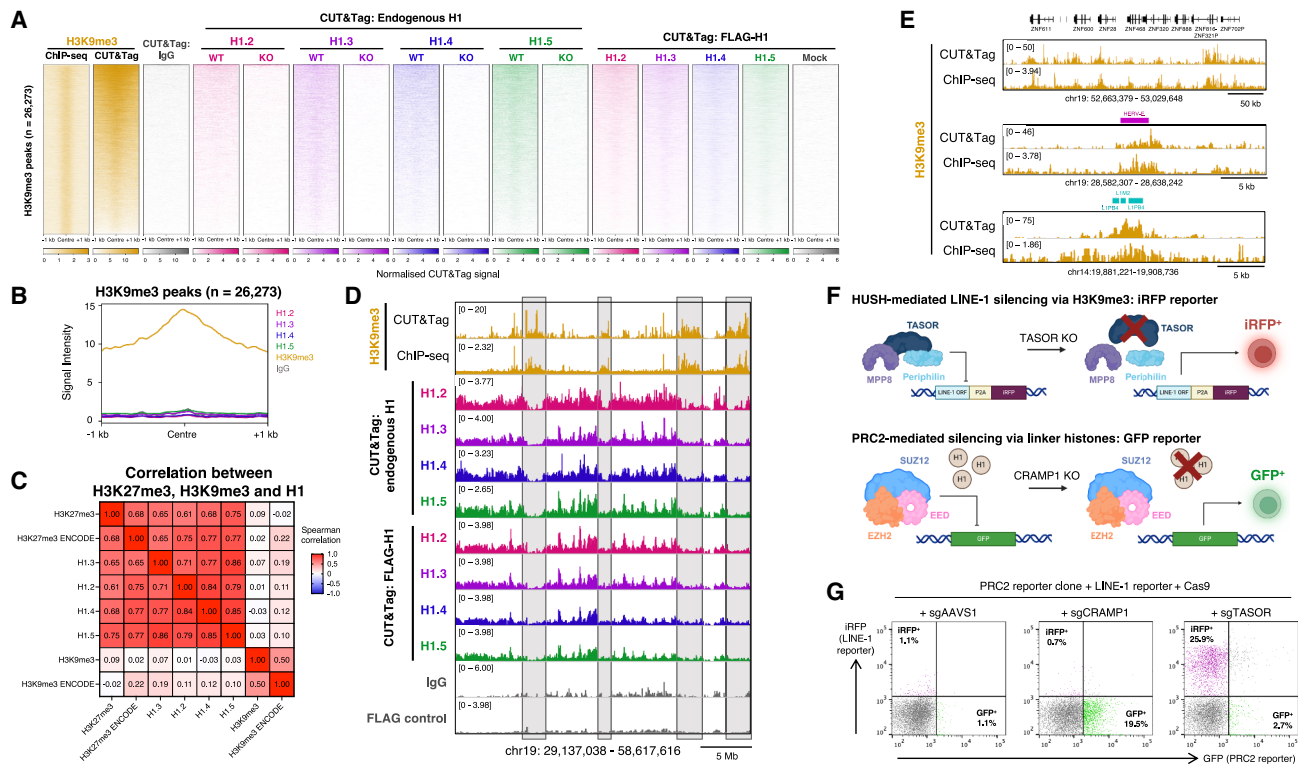


Figure 5. Linker histones are not enriched at regions marked by H3K9me3

(A–D) Lack of linker histone enrichment at H3K9me3-marked genomic regions. (A) Tornado plots depicting linker histone CUT&Tag signal across H3K9me3 peaks from the ENCODE project; average signal intensity is shown in (B). (C) Heatmap depicting the lack of correlation between linker histone occupancy and H3K9me3. Cells are annotated with pairwise Spearman correlation coefficients. An example locus is shown in (D).

(E) CUT&Tag faithfully profiles H3K9me3. Example loci comparing CUT&Tag versus H3K9me3 ChIP-seq data (ENCODE) are shown.

(F and G) Linker histone insufficiency does not impair H3K9me3-dependent LINE-1 silencing by the HUSH complex and linker histone-mediated PRC2-reporter repression. (F) Schematic representation of the dual-color reporter cell line designed to monitor both H3K9me3-dependent repression by the HUSH complex and linker histone-mediated PRC2-reporter repression. (G) HUSH-mediated LINE-1 silencing is unaffected upon CRAMP1 depletion. The indicated CRISPR sgRNAs were expressed in the dual-color reporter cell line, and GFP and iRFP fluorescence assayed by flow cytometry.

See also Figure S5 and Table S2.

histones are not a general feature of heterochromatin but instead are predominantly associated with chromatin marked by H3K27me3.

Linker histones are essential for transcriptional repression by PRC2

Given the enrichment of linker histones at genomic loci marked by H3K27me3, we hypothesized that H1 insufficiency would result in the derepression of PRC2 target genes. Global depletion of linker histones is hindered by the existence of multiple H1 subtypes and variants but can be readily achieved upon CRAMP1 ablation. RNA-seq analysis in K562 cells revealed that depletion of either CRAMP1 or the PRC2 subunit SUZ12 (Figures 6A, 6B, and S2E) resulted in the upregulation of >1,000 genes (Figure 6C; Table S8), a substantial proportion of which were shared: 58% of the genes upregulated upon CRAMP1 depletion were also derepressed upon SUZ12 depletion (Figures 6D and 6E). Moreover, the genes upregulated upon depletion of either CRAMP1 or SUZ12 were significantly enriched for H3K27me3 (Figures 6F and 6G) and were functionally enriched for developmental processes (Figure 6H). Similar results were obtained us-

ing CRISPR-Cas9-mediated gene disruption in KBM-7 cells, where 59% of the genes upregulated in CRAMP1 KO cells were also derepressed in SUZ12 KO cells (Figures S6A–S6E; Table S9). We conclude that the CRAMP1-mediated expression of linker histones is particularly important for PRC2-mediated repression.

Linker histones are required for chromatin compaction at PRC2 target sites

To explore the mechanistic requirement for histone H1 in PRC2-mediated repression, we sought to examine the molecular defects at PRC2 target genes upon ablation of CRAMP1. PRC2 recruitment to target sites did not seem to be affected by decreased levels of histone H1, as SUZ12 occupancy remained unchanged (Figures 6I, 6K, S6F–S6H, and S6L). Moreover, in contrast to cells depleted of SUZ12, shRNA-mediated depletion of CRAMP1 did not result in a reduction of H3K27me3 levels (Figures 6J, 6K, and S6I–S6L). Thus, a ~50% reduction in overall histone H1 levels following CRAMP1 loss (Figures 3B and S2E) is sufficient to derepress PRC2 target genes without concomitant loss of SUZ12 occupancy or PRC2 enzymatic activity.

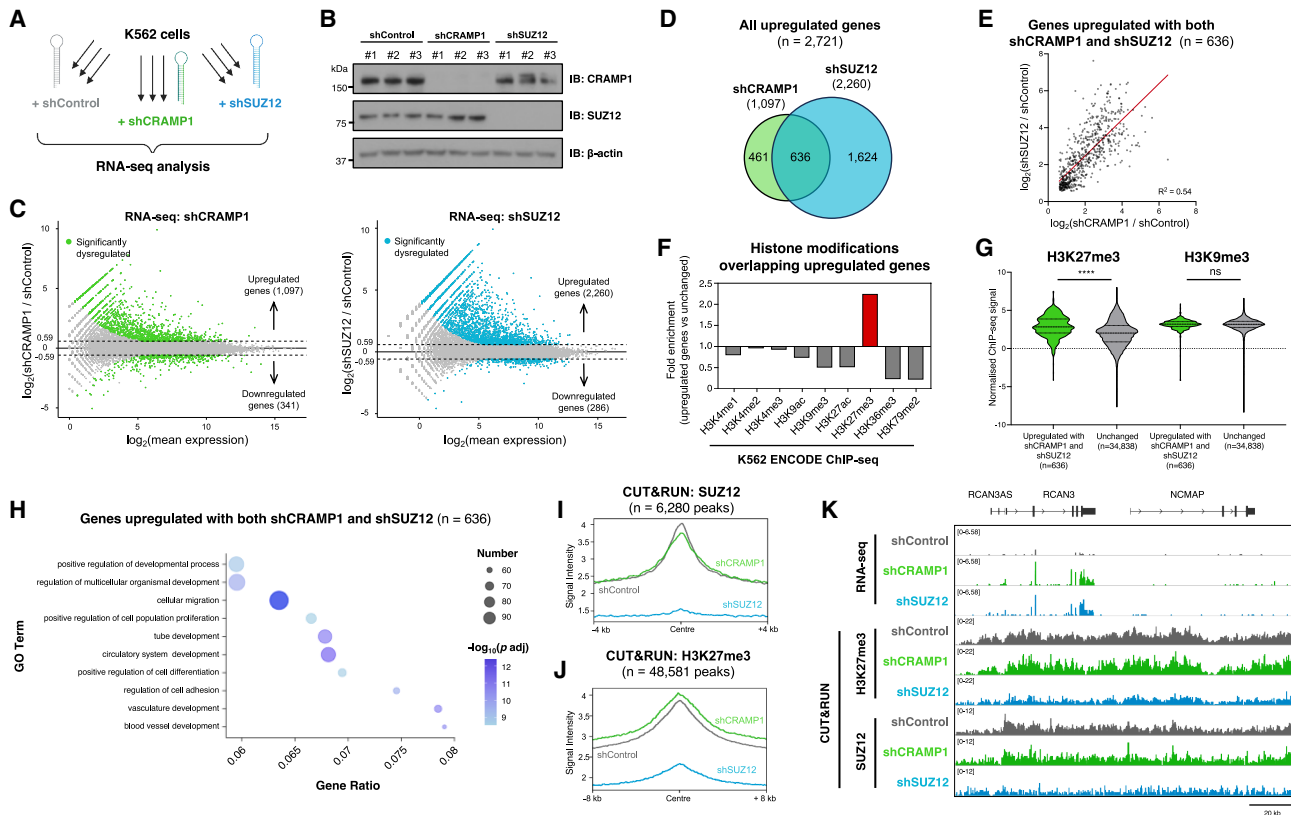


Figure 6. Loss of linker histones upon CRAMP1 ablation results in derepression of PRC2 target genes

(A) Schematic representation of the RNA-seq experiment. K562 cells were transduced in triplicate with a non-targeting shRNA (shControl) or shRNAs targeting CRAMP1 or SUZ12, followed by total RNA-seq.
 (B) Efficient shRNA-mediated depletion of CRAMP1 and SUZ12 as assessed by immunoblot.
 (C–E) Depletion of either CRAMP1 or SUZ12 results in concordant transcriptional derepression. (C) RNA-seq analysis of K562 cells depleted of CRAMP1 or SUZ12. Colored dots represent significantly dysregulated genes (DESeq2: $p < 0.05$, fold change > 1.5 or < 0.67). The overlap between the significantly upregulated genes is depicted as a Venn diagram in (D), with the relationship between the magnitude of upregulation displayed in (E).
 (F and G) Genes concordantly upregulated upon loss of CRAMP1 or SUZ12 are marked by H3K27me3. The number of histone modification peaks was enumerated across genes (± 5 kb) significantly upregulated with both shCRAMP1 and shSUZ12 ($n = 636$) versus all other genes ($n = 34,823$) (F), and violin plots represent the distribution of H3K27me3 versus H3K9me3 ChIP-seq signal across the indicated gene groups (G). (**** $p < 0.0001$; unpaired t test).
 (H) Genes upregulated upon depletion of both CRAMP1 and SUZ12 are functionally enriched for developmental processes, as assessed by Gene Ontology (GO) term analysis. Gene ratio represents the number of genes within the query term as a proportion of the total number of genes.
 (I–K) PRC2 occupancy and enzymatic activity remain unaffected upon CRAMP1 depletion. CUT&RUN analysis for SUZ12 (I) and H3K27me3 (J) reveals a decrease in signal intensity upon knockdown of SUZ12 but not CRAMP1. An example locus is shown in (K).
 See also [Figure S6](#) and [Tables S2](#), [S8](#), and [S9](#).

As linker histones condense nucleosome arrays *in vitro*,^{2,3} we wondered whether a failure of chromatin compaction at PRC2 target sites underlies the transcriptional derepression observed following CRAMP1 loss. Therefore, we employed assay for transposase-accessible chromatin using sequencing (ATAC-seq)⁵⁵ to assess changes in chromatin accessibility in cells depleted of either CRAMP1 or SUZ12 ([Figure S7A](#)). This analysis revealed a concordant increase in accessibility upon either CRAMP1 or SUZ12 knockdown across thousands of genomic loci ([Figures 7A–7C](#) and [S7B–S7H](#); [Table S10](#)). Strikingly, increased accessibility was most prominent at genomic regions marked by H3K27me3 ([Figures 7D](#) and [7E](#)). Thus, a reduction in linker histone expression following CRAMP1 depletion results in chromatin decompaction across PRC2 target sites.

DISCUSSION

By characterizing CRAMP1 as an essential regulator of linker histone gene expression, we have uncovered CRAMP1 ablation as a genetic strategy through which to interrogate the function of linker histones. Simultaneous depletion of all linker histones results in derepression of PRC2 target genes without affecting SUZ12 localization or H3K27me3 levels. Thus, our data suggest that linker histones play a more prominent role in repression at Polycomb target sites than at other repressed genomic regions.

While histone H1 appears to compact nucleosome arrays into the 30 nm fiber indiscriminately *in vitro*,^{2,3} we found that H1 subtypes are not uniformly localized throughout the genome but rather closely mimic the distribution of H3K27me3. Profiling the

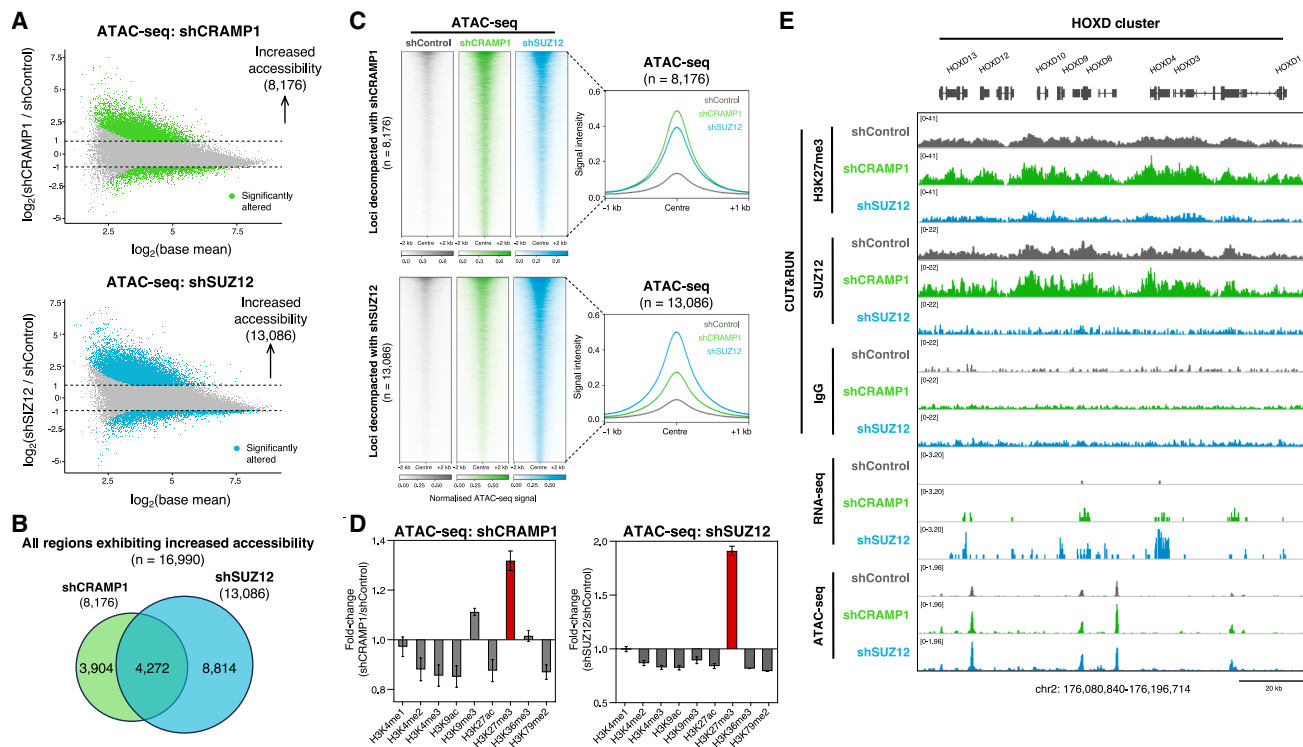


Figure 7. Loss of linker histones following CRAMP1 ablation increases the accessibility of genomic loci marked by H3K27me3

(A–C) Depletion of CRAMP1 or SUZ12 results in concordant decompaction of genomic loci. (A) K562 cells depleted of CRAMP1 or SUZ12 by shRNA-mediated knockdown were analyzed by ATAC-seq. Colored dots represent sites exhibiting a significant change in accessibility ($p < 0.05$, fold change > 2 or < 0.5). The overlap between the loci exhibiting significantly increased accessibility is depicted as a Venn diagram in (B). The relationship between the extent of decompaction in each case is displayed as a tornado plot in (C), with the average signal intensity shown on the right. (D and E) Genomic loci exhibiting increased accessibility upon loss of CRAMP1 or SUZ12 are enriched for H3K27me3. (D) Quantification of ATAC-seq signal across histone modification peaks. Increased accessibility is observed across loci marked by H3K27me3. Plots show median \pm SD of two technical replicates. The HOXD cluster is shown as an example in (E). See also [Figure S7](#) and [Table S10](#).

genome-wide occupancy of histone H1 subtypes and variants poses a unique challenge owing to the need to preserve the integrity of the linker DNA where H1 is bound. However, although CUT&Tag may be particularly well-suited to profiling linker histone localization because it does not require linker DNA fragmentation, we found that the *C. elegans* histone H1 variant HIS-24 was distributed analogously when profiled by ChIP-seq. The localization of linker histones at H3K27me3 sites is concordant with the specific derepression of Polycomb target genes observed upon H1 KO in mice^{21,24} and upon CRAMP1 depletion in human cells ([Figures 6](#) and [S6](#)). It will be interesting to determine whether linker histones are similarly required for the function of PRC2 subcomplexes beyond PRC2.1 harboring MTF2; furthermore, recent studies propose a functional link between histone H1 and H2A ubiquitination,^{56,57} suggesting that linker histones may also be required for PRC1-mediated repression. Intriguingly, CRAMP1 mutant flies also exhibit Polycomb phenotypes,⁵⁸ suggesting that the requirement for linker histones for Polycomb repression is evolutionarily conserved.

Establishing how H1 localizes to PRC2 target sites will be a priority for future investigation. Given that SUZ12 remains bound to its genomic target sites upon CRAMP1 depletion, one possibility

is that PRC2 (or H3K27me3) recruits linker histones to its target sites. Alternatively, other factors could be responsible for H1 deposition. Multiple chaperones are known to regulate the genomic distribution of core histones,⁵⁹ and thus a hitherto unidentified H1-specific chaperone could specify the localization of linker histones.

Although linker histones stimulate the methyltransferase activity of PRC2 *in vitro*^{24,49,60,61} and double and triple H1 KO cells display reduced levels of H3K27me3,^{15,21,24,49} our data do not support H3K27me3 deposition as the primary mechanism through which linker histones contribute to PRC2-mediated repression: depletion of linker histones following CRAMP1 ablation prevents PRC2-mediated repression without affecting H3K27me3 levels. One possible explanation for this discrepancy is that we have measured the short-term effects of linker histone insufficiency rather than the long-term consequences resulting from the KO of multiple H1 subtypes.

Further work will be required to establish the molecular mechanism through which CRAMP1 activates histone gene expression. CRAMP1 does not possess an annotated DNA-binding domain, suggesting that its localization to histone gene promoters is likely achieved through its interacting partners. Indeed,

we identify an interaction between CRAMP1 and two known regulators of histone expression, NPAT and GON4L, suggesting that these three proteins may act in concert to drive linker histone expression. A goal for future work will be to define the mechanistic basis for these effects. By contrast, we did not observe an interaction between CRAMP1 and FLASH, a protein that regulates 3' end processing of histone transcripts. Given that we also did not observe 3' end processing defects by RNA-seq, we speculate that CRAMP1 acts together with NPAT and GON4L to promote transcription of linker histone genes. Intriguingly, although CRAMP1 localizes to the promoters of all five families of histone genes, its loss selectively impairs the expression of linker histones. This finding mirrors observations in *Drosophila*, where the orthologous protein CRAMPED specifically regulates histone H1 expression.⁶² Future studies will need to determine how this specificity is achieved. Perhaps CRAMP1 cooperates with other factors that are exclusively localized to linker histone genes, or potentially, it could act similarly at core histone genes but in a manner redundant with other histone gene regulators.

Despite the high degree of sequence similarity between the eleven H1 subtypes and variants encoded in the human genome,⁴ an intriguing question concerns whether they have the capacity to play specific functional roles. Our data provide evidence both for and against this idea. On the one hand, simply the overall abundance of linker histones may be the limiting factor for PRC2-mediated repression. Lentiviral delivery of H1X, which displays the lowest degree of sequence similarity to other linker histones,⁴ afforded by far the highest levels of expression among all the linker histones tested in our reporter re-repression assay (Figures 3E, S2H, and S2I) and was the only one to fully restore GFP silencing (Figure S2H). However, abundance alone cannot explain all the variation in H1 activity that we observed: histone H1.4 and H1.5, for example, exhibit 86% sequence identity, and yet, despite only modest overexpression, histone H1.4 outperformed histone H1.5 in this assay (Figures S2H and S2I). Thus, histone H1.4 may be the optimal H1 subtype for PRC2 repression in K562 cells. Intriguingly, mutations in both linker histones and EZH2, the catalytic subunit of PRC2, are commonly found in germinal center B cell lymphomas,^{21,63} with H1.4 being the most frequently mutated H1 subtype.²¹ Thus, delineating the molecular mechanisms underpinning the requirement for linker histones in PRC2 function may highlight new therapeutic avenues.

Limitations of the study

Although our genetic screening strategy identified a requirement for the hitherto uncharacterized protein CRAMP1 in PRC2-mediated repression, it may have failed to identify additional relevant genes. Our genome-wide CRISPR screen failed to reach saturation, as the core PRC2 subunits—whose ablation did result in GFP reporter derepression in individual CRISPR-mediated gene disruption experiments—did not emerge as significant hits. Thus, further work will be required to delineate the full spectrum of genes required for Polycomb repression.

Here we characterize CRAMP1 ablation as an effective strategy to achieve simultaneous depletion of all linker histone subtypes. However, although this approach appears to yield uniform

effects across all linker histone genes, the magnitude of this effect is only partial: total linker abundance falls ~2-fold. We demonstrate that this reduction is sufficient to impair PRC2-mediated repression, but more substantial depletion may be required to reveal all the critical functions of linker histones. Furthermore, for most subtypes we were only able to modestly increase linker histone supply through lentiviral transduction, and it was not possible for us to precisely match the expression levels of endogenous and exogenous epitope-tagged H1 proteins.

A potential limitation for genome-wide occupancy profiling using the CUT&Tag methodology is that signal will be restricted to genomic regions accessible to the Tn5 transposase. However, the anti-correlation that we observe between linker histones and H3K9me3 cannot be explained by an inability of the Tn5 transposase to access constitutive heterochromatin, as profiling of the H3K9me3 modification itself by CUT&Tag yielded a similar distribution to that defined by a conventional ChIP-seq approach. Indeed, we consider that CUT&Tag is likely to be the optimal technique to profile H1 occupancy, as, in contrast to methods involving sonication or micrococcal nuclease digestion, CUT&Tag does not disrupt the integrity of the linker DNA.

RESOURCE AVAILABILITY

Lead contact

Further information and requests for resources and reagents should be directed to the lead contact, Iva Tchasovnikarova (it257@cam.ac.uk).

Materials availability

Resources generated in this study will be shared by the lead contact upon reasonable request.

Data and code availability

All sequencing data generated in this study have been deposited to GEO (GEO: GSE276912) and are publicly available as of the date of publication. Accession numbers for specific experiments are listed in the [key resources table](#).

This paper does not report original code. Standard bioinformatics approaches used to analyze the data are described in relevant [STAR Methods](#) sections.

Any additional information required to reanalyze the data reported in this paper is available from the [lead contact](#) upon request.

ACKNOWLEDGMENTS

We thank Joana Cerveira and her team at the School of Biological Sciences Flow Cytometry Core Facility and Kay Harnish at the Gurdon Institute NGS Facility. We are grateful to Bob Kingston and Robert Schneider for critical reading of the manuscript. This work was supported by a PhD studentship sponsored by the Gurdon Institute and Peterhouse to R.E.M. and a Cancer Research UK Cambridge Centre studentship to J.M.C.D. Research in the Tchasovnikarova laboratory is supported by Wellcome (092096) and Cancer Research UK (C6946/A14492).

AUTHOR CONTRIBUTIONS

Conceptualization, I.A.T.; methodology, R.E.M. and I.A.T.; investigation, R.E.M., E.L.N., J.M.C.D., L.E.F.S., S.L., A.A., T.B., O.S., J.S., R.A., and I.A.T.; formal analysis, R.E.M., E.L.N., J.M.C.D., A.G., A.V., F.C., A.J.R., R.A., R.T.T., and I.A.T.; writing – original draft, R.E.M. and I.A.T.; writing – review & editing, R.E.M.,

M.A.D., R.T.T., J.A., and I.A.T.; supervision, A.J.R., M.A.D., B.B., J.A., and I.A.T.; funding acquisition, R.E.M., J.M.C.D., B.B., J.A., and I.A.T.

DECLARATION OF INTERESTS

The authors declare no competing interests.

STAR★METHODS

Detailed methods are provided in the online version of this paper and include the following:

- **KEY RESOURCES TABLE**
- **EXPERIMENTAL MODEL AND STUDY PARTICIPANT DETAILS**
 - Cell culture
- **METHOD DETAILS**
 - Generation of lentiviral expression vectors
 - Lentivirus production
 - CRISPR/Cas9 screen
 - Flow cytometry
 - Immunoblotting
 - Co-immunoprecipitation
 - Mass spectrometry analysis
 - Subcellular fractionation
 - CRISPR/Cas9-mediated gene disruption
 - shRNA-mediated knockdown
 - RT-qPCR
 - RNA-seq
 - CUT&RUN
 - CUT&Tag
 - ChIP-seq
 - ATAC-seq
 - AlphaFold 3 structural prediction
- **QUANTIFICATION AND STATISTICAL ANALYSIS**
 - CRISPR/Cas9 genetic screen
 - RNA-seq
 - CUT&RUN
 - CUT&Tag
 - ChIP-seq
 - ATAC-seq

SUPPLEMENTAL INFORMATION

Supplemental information can be found online at <https://doi.org/10.1016/j.molcel.2025.05.031>.

Received: October 28, 2024

Revised: March 24, 2025

Accepted: May 22, 2025

Published: June 13, 2025

REFERENCES

1. Oudet, P., Gross-Bellard, M., and Chambon, P. (1975). Electron microscopic and biochemical evidence that chromatin structure is a repeating unit. *Cell* 4, 281–300. [https://doi.org/10.1016/0092-8674\(75\)90149-x](https://doi.org/10.1016/0092-8674(75)90149-x).
2. Thoma, F., and Koller, T. (1977). Influence of histone H1 on chromatin structure. *Cell* 12, 101–107. [https://doi.org/10.1016/0092-8674\(77\)90188-x](https://doi.org/10.1016/0092-8674(77)90188-x).
3. Renz, M., Nehls, P., and Hozier, J. (1977). Involvement of histone H1 in the organization of the chromosome fiber. *Proc. Natl. Acad. Sci. USA* 74, 1879–1883. <https://doi.org/10.1073/pnas.74.5.1879>.
4. Prendergast, L., and Reinberg, D. (2021). The missing linker: emerging trends for H1 variant-specific functions. *Genes Dev.* 35, 40–58. <https://doi.org/10.1101/gad.344531.120>.
5. Sancho, M., Diani, E., Beato, M., and Jordan, A. (2008). Depletion of human histone H1 variants uncovers specific roles in gene expression and cell growth. *PLoS Genet.* 4, e1000227. <https://doi.org/10.1371/journal.pgen.1000227>.
6. Bhan, S., May, W., Warren, S.L., and Sittman, D.B. (2008). Global gene expression analysis reveals specific and redundant roles for H1 variants, H1c and H1(0), in gene expression regulation. *Gene* 414, 10–18. <https://doi.org/10.1016/j.gene.2008.01.025>.
7. Gunjan, A., and Brown, D.T. (1999). Overproduction of histone H1 variants in vivo increases basal and induced activity of the mouse mammary tumor virus promoter. *Nucleic Acids Res.* 27, 3355–3363. <https://doi.org/10.1093/nar/27.16.3355>.
8. Brown, D.T., Alexander, B.T., and Sittman, D.B. (1996). Differential effect of H1 variant overexpression on cell cycle progression and gene expression. *Nucleic Acids Res.* 24, 486–493. <https://doi.org/10.1093/nar/24.3.486>.
9. Izzo, A., Kamieniarz-Gdula, K., Ramírez, F., Noureen, N., Kind, J., Manke, T., van Steensel, B., and Schneider, R. (2013). The genomic landscape of the somatic linker histone subtypes H1.1 to H1.5 in human cells. *Cell Rep.* 3, 2142–2154. <https://doi.org/10.1016/j.celrep.2013.05.003>.
10. Hu, S., Chapski, D.J., Gehred, N.D., Kimball, T.H., Gromova, T., Flores, A., Rowat, A.C., Chen, J., Packard, R.R.S., Olszewski, E., et al. (2024). Histone H1.0 couples cellular mechanical behaviors to chromatin structure. *Nat. Cardiovasc. Res.* 3, 441–459. <https://doi.org/10.1038/s44161-024-00460-w>.
11. Harris, C.J., Zhong, Z., Ichino, L., Feng, S., and Jacobsen, S.E. (2024). H1 restricts euchromatin-associated methylation pathways from heterochromatic encroachment. *eLife* 12, RP89353. <https://doi.org/10.7554/eLife.89353>.
12. Ito-Ishida, A., Yamalanchili, H.K., Shao, Y., Baker, S.A., Heckman, L.D., Lavery, L.A., Kim, J.-Y., Lombardi, L.M., Sun, Y., Liu, Z., et al. (2018). Genome-wide distribution of linker histone H1.0 is independent of MeCP2. *Nat. Neurosci.* 21, 794–798. <https://doi.org/10.1038/s41593-018-0155-8>.
13. Mayor, R., Izquierdo-Bouldstridge, A., Millán-Ariño, L., Bustillos, A., Sampaio, C., Luque, N., and Jordan, A. (2015). Genome distribution of replication-independent histone H1 variants shows H1.0 associated with nucleolar domains and H1X associated with RNA polymerase II-enriched regions. *J. Biol. Chem.* 290, 7474–7491. <https://doi.org/10.1074/jbc.M114.617324>.
14. Millán-Ariño, L., Islam, A.B.M.M.K., Izquierdo-Bouldstridge, A., Mayor, R., Terme, J.-M., Luque, N., Sancho, M., López-Bigas, N., and Jordan, A. (2014). Mapping of six somatic linker histone H1 variants in human breast cancer cells uncovers specific features of H1.2. *Nucleic Acids Res.* 42, 4474–4493. <https://doi.org/10.1093/nar/gku079>.
15. Teano, G., Concia, L., Wolff, L., Carron, L., Biocanin, I., Adamusová, K., Fojtová, M., Bourge, M., Kramdi, A., Colot, V., et al. (2023). Histone H1 protects telomeric repeats from H3K27me3 invasion in Arabidopsis. *Cell Rep.* 42, 112894. <https://doi.org/10.1016/j.celrep.2023.112894>.
16. Serna-Pujol, N., Salinas-Pena, M., Mugjanesi, F., Le Dily, F., Marti-Renom, M.A., and Jordan, A. (2022). Coordinated changes in gene expression, H1 variant distribution and genome 3D conformation in response to H1 depletion. *Nucleic Acids Res.* 50, 3892–3910. <https://doi.org/10.1093/nar/gkac226>.
17. Teif, V.B., Gould, T.J., Clarkson, C.T., Boyd, L., Antwi, E.B., Ishaque, N., Olins, A.L., and Olins, D.E. (2020). Linker histone epitopes are hidden by in situ higher-order chromatin structure. *Epigenetics Chromatin* 13, 26. <https://doi.org/10.1186/s13072-020-00345-9>.
18. Shimada, M., Chen, W.-Y., Nakadai, T., Onikubo, T., Guermah, M., Rhodes, D., and Roeder, R.G. (2019). Gene-Specific H1 Eviction through a Transcriptional Activator→p300→NAP1→H1 Pathway. *Mol. Cell* 74, 268–283.e5. <https://doi.org/10.1016/j.molcel.2019.02.016>.

19. Hergeth, S.P., and Schneider, R. (2015). The H1 linker histones: multifunctional proteins beyond the nucleosomal core particle. *EMBO Rep.* 16, 1439–1453. <https://doi.org/10.15252/embr.201540749>.
20. Fan, Y., Sirotkin, A., Russell, R.G., Ayala, J., and Skoultchi, A.I. (2001). Individual Somatic H1 Subtypes Are Dispensable for Mouse Development Even in Mice Lacking the H1(0) Replacement Subtype. *Mol. Cell. Biol.* 21, 7933–7943. <https://doi.org/10.1128/MCB.21.23.7933-7943.2001>.
21. Yusufova, N., Kloetgen, A., Teater, M., Osunsade, A., Camarillo, J.M., Chin, C.R., Doane, A.S., Venters, B.J., Portillo-Ledesma, S., Conway, J., et al. (2021). Histone H1 loss drives lymphoma by disrupting 3D chromatin architecture. *Nature* 589, 299–305. <https://doi.org/10.1038/s41586-020-3017-y>.
22. Fan, Y., Nikitina, T., Zhao, J., Fleury, T.J., Bhattacharyya, R., Bouhassira, E.E., Stein, A., Woodcock, C.L., and Skoultchi, A.I. (2005). Histone H1 depletion in mammals alters global chromatin structure but causes specific changes in gene regulation. *Cell* 123, 1199–1212. <https://doi.org/10.1016/j.cell.2005.10.028>.
23. Fan, Y., Nikitina, T., Morin-Kensicki, E.M., Zhao, J., Magnuson, T.R., Woodcock, C.L., and Skoultchi, A.I. (2003). H1 Linker Histones Are Essential for Mouse Development and Affect Nucleosome Spacing In Vivo. *Mol. Cell. Biol.* 23, 4559–4572. <https://doi.org/10.1128/MCB.23.13.4559-4572.2003>.
24. Willcockson, M.A., Heaton, S.E., Weiss, C.N., Bartholdy, B.A., Botbol, Y., Mishra, L.N., Sidhwani, D.S., Wilson, T.J., Pinto, H.B., Maron, M.I., et al. (2021). H1 histones control the epigenetic landscape by local chromatin compaction. *Nature* 589, 293–298. <https://doi.org/10.1038/s41586-020-3032-z>.
25. Kim, J.J., and Kingston, R.E. (2022). Context-specific Polycomb mechanisms in development. *Nat. Rev. Genet.* 23, 680–695. <https://doi.org/10.1038/s41576-022-00499-0>.
26. de Napoles, M., Mermoud, J.E., Wakao, R., Tang, Y.A., Endoh, M., Appanah, R., Nesterova, T.B., Silva, J., Otte, A.P., Vidal, M., et al. (2004). Polycomb group proteins Ring1A/B link ubiquitylation of histone H2A to heritable gene silencing and X inactivation. *Dev. Cell* 7, 663–676. <https://doi.org/10.1016/j.devcel.2004.10.005>.
27. Wang, H., Wang, L., Erdjument-Bromage, H., Vidal, M., Tempst, P., Jones, R.S., and Zhang, Y. (2004). Role of histone H2A ubiquitination in Polycomb silencing. *Nature* 431, 873–878. <https://doi.org/10.1038/nature02985>.
28. Francis, N.J., Kingston, R.E., and Woodcock, C.L. (2004). Chromatin compaction by a polycomb group protein complex. *Science* 306, 1574–1577. <https://doi.org/10.1126/science.1100576>.
29. Grau, D.J., Chapman, B.A., Garlick, J.D., Borowsky, M., Francis, N.J., and Kingston, R.E. (2011). Compaction of chromatin by diverse Polycomb group proteins requires localized regions of high charge. *Genes Dev.* 25, 2210–2221. <https://doi.org/10.1101/gad.17288211>.
30. Cao, R., Wang, L., Wang, H., Xia, L., Erdjument-Bromage, H., Tempst, P., Jones, R.S., and Zhang, Y. (2002). Role of histone H3 lysine 27 methylation in Polycomb-group silencing. *Science* 298, 1039–1043. <https://doi.org/10.1126/science.1076997>.
31. Czermin, B., Melfi, R., McCabe, D., Seitz, V., Imhof, A., and Pirrotta, V. (2002). Drosophila enhancer of Zeste/ESC complexes have a histone H3 methyltransferase activity that marks chromosomal Polycomb sites. *Cell* 111, 185–196. [https://doi.org/10.1016/s0092-8674\(02\)00975-3](https://doi.org/10.1016/s0092-8674(02)00975-3).
32. Kuzmichev, A., Nishioka, K., Erdjument-Bromage, H., Tempst, P., and Reinberg, D. (2002). Histone methyltransferase activity associated with a human multiprotein complex containing the Enhancer of Zeste protein. *Genes Dev.* 16, 2893–2905. <https://doi.org/10.1101/gad.1035902>.
33. Müller, J., Hart, C.M., Francis, N.J., Vargas, M.L., SenGupta, A., Wild, B., Miller, E.L., O'Connor, M.B., Kingston, R.E., and Simon, J.A. (2002). Histone methyltransferase activity of a Drosophila Polycomb group repressor complex. *Cell* 111, 197–208. [https://doi.org/10.1016/s0092-8674\(02\)00976-5](https://doi.org/10.1016/s0092-8674(02)00976-5).
34. Tchasovnikarova, I.A., Marr, S.K., Damle, M., and Kingston, R.E. (2022). TRACE generates fluorescent human reporter cell lines to characterize epigenetic pathways. *Mol. Cell* 82, 479–491.e7. <https://doi.org/10.1016/j.molcel.2021.11.035>.
35. Tsherniak, A., Vazquez, F., Montgomery, P.G., Weir, B.A., Kryukov, G., Cowley, G.S., Gill, S., Harrington, W.F., Pantel, S., Krill-Burger, J.M., et al. (2017). Defining a Cancer Dependency Map. *Cell* 170, 564–576.e16. <https://doi.org/10.1016/j.cell.2017.06.010>.
36. Park, R.J., Wang, T., Koundakjian, D., Hultquist, J.F., Lamothe-Molina, P., Monel, B., Schumann, K., Yu, H., Krupczak, K.M., Garcia-Beltran, W., et al. (2017). A genome-wide CRISPR screen identifies a restricted set of HIV host dependency factors. *Nat. Genet.* 49, 193–203. <https://doi.org/10.1038/ng.3741>.
37. Li, W., Xu, H., Xiao, T., Cong, L., Love, M.I., Zhang, F., Irizarry, R.A., Liu, J.S., Brown, M., and Liu, X.S. (2014). MAGeCK enables robust identification of essential genes from genome-scale CRISPR/Cas9 knockout screens. *Genome Biol.* 15, 554. <https://doi.org/10.1186/s13059-014-0554-4>.
38. Zhao, J., Kennedy, B.K., Lawrence, B.D., Barbie, D.A., Matera, A.G., Fletcher, J.A., and Harlow, E. (2000). NPAT links cyclin E-Cdk2 to the regulation of replication-dependent histone gene transcription. *Genes Dev.* 14, 2283–2297. <https://doi.org/10.1101/gad.827700>.
39. Barcaroli, D., Bongiorno-Borbone, L., Terrinoni, A., Hofmann, T.G., Rossi, M., Knight, R.A., Matera, A.G., Melino, G., and De Laurenzi, V. (2006). FLASH is required for histone transcription and S-phase progression. *Proc. Natl. Acad. Sci. USA* 103, 14808–14812. <https://doi.org/10.1073/pnas.0604227103>.
40. Yang, X.C., Sabath, I., Kunduru, L., van Wijnen, A.J., Marzluff, W.F., and Dominski, Z. (2014). A conserved interaction that is essential for the biogenesis of histone locus bodies. *J. Biol. Chem.* 289, 33767–33782. <https://doi.org/10.1074/jbc.M114.616466>.
41. Yang, X.-C., Burch, B.D., Yan, Y., Marzluff, W.F., and Dominski, Z. (2009). FLASH, a proapoptotic protein involved in activation of caspase-8, is essential for 3' end processing of histone pre-mRNAs. *Mol. Cell* 36, 267–278. <https://doi.org/10.1016/j.molcel.2009.08.016>.
42. Bulchand, S., Menon, S.D., George, S.E., and Chia, W. (2010). Muscle wasted: a novel component of the Drosophila histone locus body required for muscle integrity. *J. Cell Sci.* 123, 2697–2707. <https://doi.org/10.1242/jcs.063172>.
43. Lu, P., Hankel, I.L., Hostager, B.S., Swartzendruber, J.A., Friedman, A.D., Brenton, J.L., Rothman, P.B., and Colgan, J.D. (2011). The developmental regulator protein Gon4l associates with protein YY1, co-repressor Sin3a, and histone deacetylase 1 and mediates transcriptional repression. *J. Biol. Chem.* 286, 18311–18319. <https://doi.org/10.1074/jbc.M110.133603>.
44. Ma, T., Van Tine, B.A., Wei, Y., Garrett, M.D., Nelson, D., Adams, P.D., Wang, J., Qin, J., Chow, L.T., and Harper, J.W. (2000). Cell cycle-regulated phosphorylation of p220(NPAT) by cyclin E/Cdk2 in Cajal bodies promotes histone gene transcription. *Genes Dev.* 14, 2298–2313. <https://doi.org/10.1101/gad.829500>.
45. Bongiorno-Borbone, L., De Cola, A., Vernole, P., Finos, L., Barcaroli, D., Knight, R.A., Melino, G., and De Laurenzi, V. (2008). FLASH and NPAT positive but not Coilin positive Cajal Bodies correlate with cell ploidy. *Cell Cycle* 7, 2357–2367. <https://doi.org/10.4161/cc.6344>.
46. Huttlin, E.L., Bruckner, R.J., Paulo, J.A., Cannon, J.R., Ting, L., Baltier, K., Colby, G., Gebreab, F., Gygi, M.P., Parzen, H., et al. (2017). Architecture of the human interactome defines protein communities and disease networks. *Nature* 545, 505–509. <https://doi.org/10.1038/nature22366>.
47. Bucholc, K., Skrajna, A., Adamska, K., Yang, X.-C., Krajewski, K., Poznański, J., Dadlez, M., Domiński, Z., and Zhukov, I. (2020). Structural Analysis of the SANT/Myb Domain of FLASH and YARP Proteins and Their Complex with the C-Terminal Fragment of NPAT by NMR Spectroscopy and Computer Simulations. *Int. J. Mol. Sci.* 21, 5268. <https://doi.org/10.3390/ijms21155268>.

48. Abramson, J., Adler, J., Dunger, J., Evans, R., Green, T., Pritzel, A., Ronneberger, O., Willmore, L., Ballard, A.J., Bambrick, J., et al. (2024). Accurate structure prediction of biomolecular interactions with AlphaFold 3. *Nature* 630, 493–500. <https://doi.org/10.1038/s41586-024-07487-w>.
49. Liu, C., Yu, J., Song, A., Wang, M., Hu, J., Chen, P., Zhao, J., and Li, G. (2023). Histone H1 facilitates restoration of H3K27me3 during DNA replication by chromatin compaction. *Nat. Commun.* 14, 4081. <https://doi.org/10.1038/s41467-023-39846-y>.
50. Kaya-Okur, H.S., Wu, S.J., Codomo, C.A., Pledger, E.S., Bryson, T.D., Henikoff, J.G., Ahmad, K., and Henikoff, S. (2019). CUT&Tag for efficient epigenomic profiling of small samples and single cells. *Nat. Commun.* 10, 1930. <https://doi.org/10.1038/s41467-019-09982-5>.
51. Pascal, C., Zonszain, J., Hameiri, O., Gargi-Levi, C., Lev-Maor, G., Tammer, L., Levy, T., Tarabeih, A., Roy, V.R., Ben-Salmon, S., et al. (2023). Human histone H1 variants impact splicing outcome by controlling RNA polymerase II elongation. *Mol. Cell* 83, 3801–3817.e8. <https://doi.org/10.1016/j.molcel.2023.10.003>.
52. Torres, C.M., Biran, A., Burney, M.J., Patel, H., Henser-Brownhill, T., Cohen, A.S., Li, Y., Ben-Hamo, R., Nye, E., Spencer-Dene, B., et al. (2016). The linker histone H1.0 generates epigenetic and functional intratumor heterogeneity. *Science* 353, aaf1644. <https://doi.org/10.1126/science.aaf1644>.
53. Zhang, J., Lee, D., Dhiman, V., Jiang, P., Xu, J., McGillivray, P., Yang, H., Liu, J., Meyerson, W., Clarke, D., et al. (2020). An integrative ENCODE resource for cancer genomics. *Nat. Commun.* 11, 3696. <https://doi.org/10.1038/s41467-020-14743-w>.
54. Seczynska, M., Bloor, S., Cuesta, S.M., and Lehner, P.J. (2022). Genome surveillance by HUSH-mediated silencing of intronless mobile elements. *Nature* 601, 440–445. <https://doi.org/10.1038/s41586-021-04228-1>.
55. Buenrostro, J.D., Giresi, P.G., Zaba, L.C., Chang, H.Y., and Greenleaf, W. J. (2013). Transposition of native chromatin for fast and sensitive epigenomic profiling of open chromatin, DNA-binding proteins and nucleosome position. *Nat. Methods* 10, 1213–1218. <https://doi.org/10.1038/nmeth.2688>.
56. Zhao, J., Wang, M., Chang, L., Yu, J., Song, A., Liu, C., Huang, W., Zhang, T., Wu, X., Shen, X., et al. (2020). RYBP/YAF2-PRC1 complexes and histone H1-dependent chromatin compaction mediate propagation of H2AK119ub1 during cell division. *Nat. Cell Biol.* 22, 439–452. <https://doi.org/10.1038/s41556-020-0484-1>.
57. Zhao, J., Lan, J., Wang, M., Liu, C., Fang, Z., Song, A., Zhang, T., Wang, L., Zhu, B., Chen, P., et al. (2024). H2AK119ub1 differentially fine-tunes gene expression by modulating canonical PRC1- and H1-dependent chromatin compaction. *Mol. Cell* 84, 1191–1205.e7. <https://doi.org/10.1016/j.molcel.2024.02.017>.
58. Yamamoto, Y., Girard, F., Bello, B., Affolter, M., and Gehring, W.J. (1997). The cramped gene of *Drosophila* is a member of the Polycomb-group, and interacts with *mus209*, the gene encoding Proliferating Cell Nuclear Antigen. *Development* 124, 3385–3394. <https://doi.org/10.1242/dev.124.17.3385>.
59. Hammond, C.M., Strömme, C.B., Huang, H., Patel, D.J., and Groth, A. (2017). Histone chaperone networks shaping chromatin function. *Nat. Rev. Mol. Cell Biol.* 18, 141–158. <https://doi.org/10.1038/nrm.2016.159>.
60. Yuan, W., Wu, T., Fu, H., Dai, C., Wu, H., Liu, N., Li, X., Xu, M., Zhang, Z., Niu, T., et al. (2012). Dense chromatin activates Polycomb repressive complex 2 to regulate H3 lysine 27 methylation. *Science* 337, 971–975. <https://doi.org/10.1126/science.1225237>.
61. Martin, C., Cao, R., and Zhang, Y. (2006). Substrate preferences of the EZH2 histone methyltransferase complex. *J. Biol. Chem.* 281, 8365–8370. <https://doi.org/10.1074/jbc.M513425200>.
62. Gibert, J.M., and Karch, F. (2011). The Polycomb group protein CRAMPED is involved with TRF2 in the activation of the histone H1 gene. *Chromosoma* 120, 297–307. <https://doi.org/10.1007/s00412-011-0312-2>.
63. Reddy, A., Zhang, J., Davis, N.S., Moffitt, A.B., Love, C.L., Waldrop, A., Leppä, S., Pasanen, A., Meriranta, L., Karjalainen-Lindsberg, M.-L., et al. (2017). Genetic and Functional Drivers of Diffuse Large B Cell Lymphoma. *Cell* 171, 481–494.e15. <https://doi.org/10.1016/j.cell.2017.09.027>.
64. Kang, H., Shokhirev, M.N., Xu, Z., Chandran, S., Dixon, J.R., and Hetzer, M.W. (2020). Dynamic regulation of histone modifications and long-range chromosomal interactions during postmitotic transcriptional reactivation. *Genes Dev.* 34, 913–930. <https://doi.org/10.1101/gad.335794.119>.
65. Madrazo, E., González-Novo, R., Ortiz-Placín, C., García de Lacoba, M., González-Murillo, Á., Ramírez, M., and Redondo-Muñoz, J. (2022). Fast H3K9 methylation promoted by CXCL12 contributes to nuclear changes and invasiveness of T-acute lymphoblastic leukemia cells. *Oncogene* 41, 1324–1336. <https://doi.org/10.1038/s41388-021-02168-8>.
66. Grossman, S.R., Engreitz, J., Ray, J.P., Nguyen, T.H., Hacohen, N., and Lander, E.S. (2018). Positional specificity of different transcription factor classes within enhancers. *Proc. Natl. Acad. Sci. USA* 115, E7222–E7230. <https://doi.org/10.1073/pnas.1804663115>.
67. Jänes, J., Dong, Y., Schoof, M., Serizay, J., Appert, A., Cerrato, C., Woodbury, C., Chen, R., Gemma, C., Huang, N., et al. (2018). Chromatin accessibility dynamics across *C. elegans* development and ageing. *eLife* 7, e37344. <https://doi.org/10.7554/eLife.37344>.
68. McMurphy, A.N., Stempor, P., Gaarenstroom, T., Wolsolmerski, B., Dong, Y., Aushianikava, D., Appert, A., Huang, N., Kolasinska-Zwierz, P., Sapetschnig, A., et al. (2017). A team of heterochromatin factors collaborates with small RNA pathways to combat repetitive elements and germline stress. *eLife* 6, e21666. <https://doi.org/10.7554/eLife.21666>.
69. Tchasonnikarova, I.A., Timms, R.T., Douse, C.H., Roberts, R.C., Dougan, G., Kingston, R.E., Modis, Y., and Lehner, P.J. (2017). Hyperactivation of HUSH complex function by Charcot-Marie-Tooth disease mutation in MORC2. *Nat. Genet.* 49, 1035–1044. <https://doi.org/10.1038/ng.3878>.
70. Brinkman, E.K., and van SteENSEL, B. (2019). Rapid Quantitative Evaluation of CRISPR Genome Editing by TIDE and TIDER. *Methods Mol. Biol.* 1961, 29–44. https://doi.org/10.1007/978-1-4939-9170-9_3.
71. Robinson, J.T., Thorvaldsdóttir, H., Winckler, W., Guttman, M., Lander, E. S., Getz, G., and Mesirov, J.P. (2011). Integrative genomics viewer. *Nat. Biotechnol.* 29, 24–26. <https://doi.org/10.1038/nbt.1754>.
72. Heinz, S., Benner, C., Spann, N., Bertolino, E., Lin, Y.C., Laslo, P., Cheng, J.X., Murre, C., Singh, H., and Glass, C.K. (2010). Simple combinations of lineage-determining transcription factors prime cis-regulatory elements required for macrophage and B cell identities. *Mol. Cell* 38, 576–589. <https://doi.org/10.1016/j.molcel.2010.05.004>.
73. Ramírez, F., Ryan, D.P., Grüning, B., Bhardwaj, V., Kilpert, F., Richter, A. S., Heyne, S., Dündar, F., and Manke, T. (2016). deepTools2: a next generation web server for deep-sequencing data analysis. *Nucleic Acids Res.* 44, W160–W165. <https://doi.org/10.1093/nar/gkw257>.
74. Kolberg, L., Raudvere, U., Kuzmin, I., Adler, P., Vilo, J., and Peterson, H. (2023). g:Profiler-interoperable web service for functional enrichment analysis and gene identifier mapping (2023 update). *Nucleic Acids Res.* 51, W207–W212. <https://doi.org/10.1093/nar/gkad347>.
75. Quinlan, A.R., and Hall, I.M. (2010). BEDTools: a flexible suite of utilities for comparing genomic features. *Bioinformatics* 26, 841–842. <https://doi.org/10.1093/bioinformatics/btq033>.
76. Langmead, B., and Salzberg, S.L. (2012). Fast gapped-read alignment with Bowtie 2. *Nat. Methods* 9, 357–359. <https://doi.org/10.1038/nmeth.1923>.
77. Love, M.I., Huber, W., and Anders, S. (2014). Moderated estimation of fold change and dispersion for RNA-seq data with DESeq2. *Genome Biol.* 15, 550. <https://doi.org/10.1186/s13059-014-0550-8>.
78. Pettersen, E.F., Goddard, T.D., Huang, C.C., Meng, E.C., Couch, G.S., Croll, T.I., Morris, J.H., and Ferrin, T.E. (2021). UCSF ChimeraX: Structure visualization for researchers, educators, and developers. *Protein Sci.* 30, 70–82. <https://doi.org/10.1002/pro.3943>.

79. Pasini, D., Bracken, A.P., Jensen, M.R., Lazznerini Denchi, E., and Helin, K. (2004). Suz12 is essential for mouse development and for EZH2 histone methyltransferase activity. *EMBO J.* **23**, 4061–4071. <https://doi.org/10.1038/sj.emboj.7600402>.
80. Tzelepis, K., Koike-Yusa, H., De Braekeleer, E., Li, Y., Metzakopian, E., Dovey, O.M., Mupo, A., Grinkevich, V., Li, M., Mazan, M., et al. (2016). A CRISPR Dropout Screen Identifies Genetic Vulnerabilities and Therapeutic Targets in Acute Myeloid Leukemia. *Cell Rep.* **17**, 1193–1205. <https://doi.org/10.1016/j.celrep.2016.09.079>.
81. Wang, T., Birsoy, K., Hughes, N.W., Krupczak, K.M., Post, Y., Wei, J.J., Lander, E.S., and Sabatini, D.M. (2015). Identification and characterization of essential genes in the human genome. *Science* **350**, 1096–1101. <https://doi.org/10.1126/science.aac7041>.
82. Doench, J.G., Fusi, N., Sullender, M., Hegde, M., Vaimberg, E.W., Donovan, K.F., Smith, I., Tothova, Z., Wilen, C., Orchard, R., et al. (2016). Optimized sgRNA design to maximize activity and minimize off-target effects of CRISPR-Cas9. *Nat. Biotechnol.* **34**, 184–191. <https://doi.org/10.1038/nbt.3437>.
83. Tchasovnikarova, I.A., Timms, R.T., Matheson, N.J., Wals, K., Antrobus, R., Göttgens, B., Dougan, G., Dawson, M.A., and Lehner, P.J. (2015). GENE SILENCING. Epigenetic silencing by the HUSH complex mediates position-effect variegation in human cells. *Science* **348**, 1481–1485. <https://doi.org/10.1126/science.aaa7227>.
84. Brenner, S. (1974). The genetics of *Caenorhabditis elegans*. *Genetics* **77**, 71–94. <https://doi.org/10.1093/genetics/77.1.71>.
85. Martin, M. (2011). Cutadapt removes adapter sequences from high-throughput sequencing reads. *EMBnet J.* **17**, 10. <https://doi.org/10.14806/ej.17.1.200>.
86. Zhang, Y., Liu, T., Meyer, C.A., Eeckhoute, J., Johnson, D.S., Bernstein, B. E., Nusbaum, C., Myers, R.M., Brown, M., Li, W., et al. (2008). Model-based analysis of ChIP-Seq (MACS). *Genome Biol.* **9**, R137. <https://doi.org/10.1186/gb-2008-9-9-r137>.
87. Nassar, L.R., Barber, G.P., Benet-Pagès, A., Casper, J., Clawson, H., Diekhans, M., Fischer, C., Gonzalez, J.N., Hinrichs, A.S., Lee, B.T., et al. (2023). The UCSC Genome Browser database: 2023 update. *Nucleic Acids Res.* **51**, D1188–D1195. <https://doi.org/10.1093/nar/gkac1072>.
88. Gschwind, A.R., Mualim, K.S., Karbalayghareh, A., Sheth, M.U., Dey, K.K., Jagoda, E., Nurtdinov, R.N., Xi, W., Tan, A.S., Jones, H., et al. (2023). An encyclopedia of enhancer-gene regulatory interactions in the human genome. Preprint at bioRxiv. <https://doi.org/10.1101/2023.11.09.563812>.

STAR★METHODS

KEY RESOURCES TABLE

REAGENT or RESOURCE	SOURCE	IDENTIFIER
Antibodies		
rabbit α -CRAMP1 (used for immunoblot)	Atlas Antibodies	Cat#HPA041752; RRID:AB_10796459
rabbit α -CRAMP1(used for IP and CUT&RUN)	Fortis Life Sciences	Cat#A304-094A; RRID:AB_2621343
mouse α -Tubulin	Cell Signaling Technologies	Cat#3873; RRID:AB_1904178
rabbit α -GAPDH	Cell Signaling Technologies	Cat#2118; RRID:AB_561053
rabbit α -HP1 α	Cell Signaling Technologies	Cat#2616; RRID:AB_2070987
rabbit α -H1.0	Proteintech	Cat#17510-1-AP; RRID:AB_10695628
rabbit α -H1.1	Abcam	Cat#ab254394; RRID:AB_3677544
rabbit α -H1.2	Proteintech	Cat#19649-1-AP; RRID:AB_10694432
rabbit α -H1.3	BioRad	Cat#VPA00783; RRID:AB_3677545
rabbit α -H1.4	Cell Signaling Technologies	Cat#41328; RRID:AB_2799199
rabbit α -H1.5	Abcam	Cat#ab18208; RRID:AB_470263
rabbit α -H1X	Fortis Life Sciences	Cat#A304-604A; RRID:AB_2620799
mouse α - β -actin	Merck	Cat#A2228; RRID:AB_476697
rabbit α -H2A	Active Motif	Cat#39235; RRID:AB_2687477
mouse α -H2B	Abcam	Cat#52484; RRID:AB_1139809
rabbit α -H3	Cell Signaling Technologies	Cat#4499; RRID:AB_10544537
mouse α -H4	Abcam	Cat#ab17036; RRID:AB_1209245
rabbit α -SUZ12	Proteintech	Cat#20366-1-AP; RRID:AB_10694152
mouse α -FLAG	Merck	Cat#F1804; RRID:AB_262044
rabbit α -H3K27me3 (used for immunoblot)	Merck Millipore	Cat#07-449; RRID:AB_310624
rabbit α -H3K27me3 (used for CUT&RUN and CUT&Tag)	Epicyphe	Cat#13-0055; RRID:AB_3665059
mouse α -V5	Abcam	Cat#ab27671; RRID:AB_471093
rabbit α -IgG	EpiCypher	Cat#13-0042; RRID:AB_2923178
rabbit α -H3K9me3	Abcam	Cat#ab8898; RRID:AB_306848
α -HIS-24 (raised against amino acids 37-113)	This manuscript (Produced by Strategic Diagnostics International)	N/A
rabbit α -NPAT	Fortis Life Sciences	Cat#A302-772A; RRID:AB_10630262
rabbit α -GON4L	Atlas Antibodies	Cat# HPA057305; RRID:AB_2683408
Peroxidase AffiniPure Donkey Anti-Rabbit IgG (H+L)	Jackson ImmunoResearch	Cat#711-035-152; RRID:AB_10015282
Peroxidase AffiniPure Mouse Anti-Rabbit IgG (H+L)	Jackson ImmunoResearch	Cat#715-035-150; RRID:AB_2340770
Bacterial and virus strains		
NEB 5-alpha Competent E. coli	New England Biolabs	Cat#C2987
Chemicals, peptides, and recombinant proteins		
PolyJet in vitro DNA transfection reagent	SignaGen Laboratories	Cat#SL100688
Hygromycin B	Thermo Fisher Scientific	Cat#10687010
Blasticidin S HCl	Stratech	Cat#B4879
Puromycin Dihydrochloride	Thermo Fisher Scientific	Cat#A1113803
T4 Polynucleotide Kinase	New England Biolabs	Cat#M0201L
T4 DNA Ligase	New England Biolabs	Cat#M0202L
DNase I	Qiagen	Cat#79256
Pierce Protein A Magnetic Beads	Thermo Fisher Scientific	Cat#88846
Pierce Protein G Magnetic Beads	Thermo Fisher Scientific	Cat#88848

(Continued on next page)

Continued

REAGENT or RESOURCE	SOURCE	IDENTIFIER
Critical commercial assays		
NEBuilder HiFi DNA Assembly Master Mix	New England Biolabs	Cat#E2621
LunaScript RT SuperMix	New England Biolabs	Cat#M3010
Luna Universal qPCR Master Mix	New England Biolabs	Cat#M3003
RNeasy Mini kit	Qiagen	Cat#74106
CUTANA ChIC/CUT&RUN kit	EpiCypher	Cat#14-1048
CUTANA CUT&Tag kit	EpiCypher	Cat#14-1102
NEBNext Ultra II DNA Library Prep Kit for Illumina	New England Biolabs	Cat#E7645
NEBNext rRNA Depletion Kit v2	New England Biolabs	Cat#E7405
NEBNext Ultra II Directional RNA Library Prep Kit for Illumina	New England Biolabs	Cat#E7760
Deposited data		
H3K27me3 ChIP-seq in K562 cells	ENCODE	ENCFF915XIL
H3K4me1 ChIP-seq in K562 cells	ENCODE	ENCFF839DZV
H3K4me2 ChIP-seq in K562 cells	ENCODE	ENCFF446FUS
H3K4me3 ChIP-seq in K562 cells	ENCODE	ENCFF633WWH
H3K9ac ChIP-seq in K562 cells	ENCODE	ENCFF149MXA
H3K9me3 ChIP-seq in K562 cells	ENCODE	ENCFF559DHZ, ENCFF744MLH, ENCFF928ZQM
H3K27ac ChIP-seq in K562 cells	ENCODE	ENCFF232RQF
H3K27me3 ChIP-seq in K562 cells	ENCODE	ENCFF915XIL, ENCFF330YFF
H3K36me3 ChIP-seq in K562 cells	ENCODE	ENCFF925FDY
H3K79me2 ChIP-seq in K562 cells	ENCODE	ENCFF711PLM
Input ChIP-seq in K562 cells (for H3K27me3 dataset)	ENCODE	ENCFF355SGP
Input ChIP-seq in K562 cells (for all other datasets)	ENCODE	ENCFF893MMO
H3K4me1 ChIP-seq in HCT116 cells	ENCODE	ENCFF485QHQ
H3K4me2 ChIP-seq in HCT116 cells	ENCODE	ENCFF205HPZ
H3K4me3 ChIP-seq in HCT116 cells	ENCODE	ENCFF178EXO
H3K9ac ChIP-seq in HCT116 cells	ENCODE	ENCFF676ASZ
H3K9me3 ChIP-seq in HCT116 cells	ENCODE	ENCFF568HSD
H3K27ac ChIP-seq in HCT116 cells	ENCODE	ENCFF087TXL
H3K27me3 ChIP-seq in HCT116 cells	ENCODE	ENCFF271HVJ
H3K36me3 ChIP-seq in HCT116 cells	ENCODE	ENCFF412ONB
H3K79me2 ChIP-seq in HCT116 cells	ENCODE	ENCFF949CYK
H4K20me1 ChIP-seq in HCT116 cells	ENCODE	ENCFF085FNO
Input ChIP-seq in HCT116 cells	ENCODE	ENCFF373OZW
H3K4me3 peaks in RPE-1 cells	Kang et al. ⁶⁴	GSM4194686
H3K9me3 peaks in RPE-1 cells	ChIP Atlas	DRX002909
H3K27ac peaks in RPE-1 cells	Kang et al. ⁶⁴	GSM4194692
H3K4me3 peaks in Jurkat cells	ENCODE	ENCFF305JOT
H3K9me3 peaks in Jurkat cells	Madrazo et al. ⁶⁵	GSE162605
H3K27ac peaks in Jurkat cells	Grossman et al. ⁶⁶	GSE115438
H1 CUT&Tag in murine CD8 ⁺ T cells	Willcockson et al. ²⁴	GSE153543
H3K27me3 CUT&Tag in murine CD8 ⁺ T cells	Willcockson et al. ²⁴	GSE153543
H3K27me3 ChIP-seq in <i>C. elegans</i> L3 larvae	Jänes et al. ⁶⁷	GSM3141784, GSM3141785
H3K4me3 ChIP-seq in <i>C. elegans</i> L3 larvae	Jänes et al. ⁶⁷	GSM3141748
H3K36me3 ChIP-seq in <i>C. elegans</i> L3 larvae	Jänes et al. ⁶⁷	GSM3141772
Input ChIP-seq in <i>C. elegans</i> L3 larvae	McMurphy et al. ⁶⁸	GSM2333112, GSM2333111

(Continued on next page)

Continued

REAGENT or RESOURCE	SOURCE	IDENTIFIER
H1 ChIP-seq in L3 in <i>C. elegans</i> L3 larvae	This manuscript	GSE276858
H1.4 ChIP-seq in murine ESCs	Liu et al. ⁴⁹	GSM5770168
H1.0 ChIP-seq in murine cardiac fibroblasts	Hu et al. ¹⁰	GSE215266
H1.2 and H1.5 ChIP-seq in human HL-60/S4 cells	Teif et al. ¹⁷	GSE136264
CRAMP1 CUT&RUN in K562 cells	This manuscript	GSE276852
CUT&Tag in K562, HCT116, RPE1 and Jurkat cells	This manuscript	GSE276857
H3K27me3 and SUZ12 CUT&RUN in K562 cells depleted of CRAMP1 or SUZ12	This manuscript	GSE276860
H3K27me3 and SUZ12 CUT&Tag in K562 cells depleted of CRAMP1 or SUZ12	This manuscript	GSE276861
RNA-seq in K562 cells depleted of CRAMP1 or SUZ12	This manuscript	GSE276854
RNA-seq in CRAMP1 and SUZ12 knockout KBM-7 cells	This manuscript	GSE276859
ATAC-seq in K562 cells depleted of CRAMP1 or SUZ12	This manuscript	GSE276863

Experimental models: Cell lines

K562	ATCC	#CCL-243
hTERT RPE-1	ATCC	#CRL-4000
HEK-293T	Gift from Prof. Paul Lehner	N/A
KBM-7	Gift from Prof. Paul Lehner	N/A
Jurkat	Gift from Prof. Paul Lehner	N/A
HCT116	Gift from Prof. Steve Jackson	N/A

Oligonucleotides

See Table S11	This manuscript	N/A
-------------------------------	-----------------	-----

Recombinant DNA

pHRSIN-pSFFV-V5-CRAMP1-IRES-mCherry-WPRE-pPGK-Hygromycin ^R	This manuscript	N/A
pHRSIN-pSFFV-V5-CRAMP1dSANT-IRES-mCherry-WPRE-pPGK-Hygromycin ^R	This manuscript	N/A
pHRSIN-pSFFV-V5-CRAMP1dDomII-IRES-mCherry-WPRE-pPGK-Hygromycin ^R	This manuscript	N/A
pHRSIN-pSFFV-V5-CRAMP1dUBL-IRES-mCherry-WPRE-pPGK-Hygromycin ^R	This manuscript	N/A
pHRSIN-pSFFV-FLAG-H1.2-IRES-mCherry-WPRE-pPGK-Hygromycin ^R	This manuscript	N/A
pHRSIN-pSFFV-FLAG-H1.3-IRES-mCherry-WPRE-pPGK-Hygromycin ^R	This manuscript	N/A
pHRSIN-pSFFV-FLAG-H1.4-IRES-mCherry-WPRE-pPGK-Hygromycin ^R	This manuscript	N/A
pHRSIN-pSFFV-FLAG-H1.5-IRES-mCherry-WPRE-pPGK-Hygromycin ^R	This manuscript	N/A
pHRSIN-pSFFV-H1.1-IRES-mCherry-WPRE-pPGK-Hygromycin ^R	This manuscript	N/A
pHRSIN-pSFFV-H1.2-IRES-mCherry-WPRE-pPGK-Hygromycin ^R	This manuscript	N/A
pHRSIN-pSFFV-H1.3-IRES-mCherry-WPRE-pPGK-Hygromycin ^R	This manuscript	N/A
pHRSIN-pSFFV-H1.4-IRES-mCherry-WPRE-pPGK-Hygromycin ^R	This manuscript	N/A
pHRSIN-pSFFV-H1.5-IRES-mCherry-WPRE-pPGK-Hygromycin ^R	This manuscript	N/A
pHRSIN-pSFFV-H1.0-IRES-mCherry-WPRE-pPGK-Hygromycin ^R	This manuscript	N/A

(Continued on next page)

Continued

REAGENT or RESOURCE	SOURCE	IDENTIFIER
pHRSIN-pSFFV-H1X-IRES-mCherry-WPRE-pPGK-Hygromycin ^R	This manuscript	N/A
pKLV2-pSFFV-SUZ12-pPGK-Puro-2A-BFP-WPRE	This manuscript	N/A
pHRSIN-pSFFV-BFP-IRES-mCherry-WPRE-pPGK-Hygromycin ^R	This manuscript	N/A
pHRSIN-pSFFV-mCherry-IRES-mCherry-WPRE-pPGK-Hygromycin ^R	This manuscript	N/A
pHRSIN-pSFFV-V5-MORC2-IRES-mCherry-WPRE-pPGK-Hygromycin ^R	Prof. Paul Lehner; Tchasovnikarova et al. ⁶⁹	N/A
pHRSIN-pSFFV-L1-iRFP-WPRE-pSV40-Blasticidin ^R	Prof. Paul Lehner; Seczynska et al. ⁵⁴	N/A

Software and algorithms

TIDE v3.3.0	Brinkman and van Steensel ⁷⁰	https://tide.nki.nl/
Prism v9.5.1	GraphPad	https://www.graphpad.com/
SeqMonk v1.48.1	Babraham Bioinformatics Group	https://www.bioinformatics.babraham.ac.uk/projects/seqmonk/
IGV v2.16.1	Robinson et al. ⁷¹	https://igv.org/
HOMER v4.11	Heinz et al. ⁷²	http://homer.ucsd.edu/homer/motif/
deepTools v3.5.1	Ramirez et al. ⁷³ and Kolberg et al. ⁷⁴	https://deeptools.readthedocs.io/
g:Profiler	Kolberg et al. ⁷⁴	https://biit.cs.ut.ee/gprofiler/gost
Bedtools v2.27.1	Quinlan and Hall ⁷⁵	https://bedtools.readthedocs.io/
Bowtie2 v2.3.5.1	Langmead and Salzberg ⁷⁶	https://bowtie-bio.sourceforge.net/bowtie2/index.shtml
DESeq2	Love et al. ⁷⁷	https://bioconductor.org/packages/release/bioc/html/DESeq2.html
ggplot2	Hadley Wickham	https://ggplot2.tidyverse.org/
FlowJo v10.10.0	BD Biosciences	https://www.flowjo.com/
AlphaFold3	Abramson et al. ⁴⁸	https://alphafoldserver.com/
UCSF ChimeraX v1.6.1	Pettersen et al. ⁷⁸	https://www.cgl.ucsf.edu/chimerax/

EXPERIMENTAL MODEL AND STUDY PARTICIPANT DETAILS

Cell culture

K562 cells (#CCL-243) and hTERT RPE-1 (#CRL-4000) were purchased from ATCC. HEK-293T, KBM-7 and Jurkat cells were a gift from Prof. Paul Lehner (CITIID, University of Cambridge) and HCT116 cells were a gift from Prof. Steve Jackson (Cancer Research UK Cambridge Institute). KBM-7, K562 and HEK-293T cells were cultured in IMDM (ThermoFisher Scientific, #12440053), Jurkat cells were cultured in RPMI (Sigma-Aldrich, #R8758), HCT116 cells were cultured in DMEM (ThermoFisher Scientific, #11995065) and RPE-1 cells were cultured in DMEM F-12 medium (ThermoFisher Scientific, #11330032). All media was supplemented with 10% fetal bovine serum (ThermoFisher Scientific, #A5256701) and penicillin/streptomycin (100 U/ml) (ThermoFisher Scientific, #15140122). Cell lines were routinely tested for mycoplasma contamination (EZ PCR Mycoplasma Test Kit, GeneFlow).

METHOD DETAILS

Generation of lentiviral expression vectors

The lentiviral transfer plasmids pHRSIN-pSFFV-Cas9-WPRE-pPGK-Blasticidin^R and pHRSIN-pSFFV-V5-MORC2-IRES-mCherry-WPRE-pPGK-Hygromycin^R were a kind gift from Prof. Paul Lehner (CITIID, University of Cambridge).⁶⁹ CRAMP1 was amplified from K562 cDNA and cloned into pHRSIN-pSFFV-V5-MORC2-IRES-mCherry-WPRE-pPGK-Hygromycin^R in place of MORC2. H1 subtypes and variants were amplified from either K562 cDNA or genomic DNA and cloned into pHRSIN-pSFFV-V5-MORC2-IRES-mCherry-WPRE-pPGK-Hygromycin^R in place of V5-MORC2; an N-terminal FLAG tag was added for CUT&Tag experiments. SUZ12 was amplified from pCMV-HA-SUZ12 (Addgene #24232, kindly deposited by Kristian Helin⁷⁹) and cloned into the pKLV2-U6sgRNA-PGKpuro2ABFP-WPRE (Addgene #67974, kindly deposited by Kosuke Yusa⁸⁰) lentiviral vector downstream of an

SFFV promoter in place of the U6-sgRNA expression cassette. BFP and mCherry were cloned into pHRSIN-pSFFV-V5-MORC2-IRES-mCherry-WPRE-pPGK-Hygromycin^R in place of V5-MORC2 following amplification from pKLV2-U6sgRNA-PGKpur-o2ABFP-WPRE and pSFFV-V5-MORC2-IRES-mCherry-WPRE-pPGK-Hygromycin^R, respectively.

Lentivirus production

HEK-293T cells were transfected with the target lentiviral transfer plasmid plus four packaging plasmids encoding Gag-Pol, Rev, Tat and VSV-G respectively using PolyJet In Vitro DNA Transfection Reagent (SignaGen Laboratories, #SL100688). Viral supernatant was harvested at 48 h post-transfection and passed through a 0.45 μm filter. Target cells were transduced by spinoculation at 800 $\times g$ for 1 hour. Untransduced KBM-7 cells were eliminated using either 500 $\mu\text{g}/\text{ml}$ hygromycin (ThermoFisher Scientific, #10687010), 6.7 $\mu\text{g}/\text{ml}$ blasticidin (Strattech, #B4879) or 0.75 $\mu\text{g}/\text{ml}$ puromycin (ThermoFisher Scientific, #A1113803); untransduced K562 cells were eliminated using either 250 $\mu\text{g}/\text{ml}$ hygromycin, 10 $\mu\text{g}/\text{ml}$ blasticidin or 1 $\mu\text{g}/\text{ml}$ puromycin.

CRISPR/Cas9 screen

PRC2-reporter KBM-7 cells³⁴ expressing Cas9 were mutagenized using the Sabatini/Lander Human CRISPR Pooled Library (Addgene #1000000100, kindly deposited by David Sabatini and Eric Lander⁸¹) at a multiplicity of infection of ~ 0.3 . Untransduced cells were removed using puromycin commencing 48 h post-transduction. At 7 days post-transduction, GFP^{bright} cells were enriched by FACS using a FACSAria II (BD) cell sorter; a second sort to further enrich the GFP^{bright} population was carried out a further 10 days later. Genomic DNA was extracted using the Puregene Kit (Qiagen, #158043) from both the sorted cells and the unsorted library which had been grown in parallel. The sgRNA variable region was amplified by PCR (Q5 High-Fidelity Polymerase, NEB #M0493) using a pool of forward primers which bound the U6 promoter region and a reverse primer which bound the constant region of the sgRNA. The reaction products were pooled, purified using Agencourt AMPure XP beads (Beckman Coulter, #A63880), and 200 ng was used as a template for the second round of PCR, which consisted of 7 cycles using Illumina P5- and P7-adapted primers. After AMPure XP bead purification, PCR products were quantified using a Nanodrop spectrophotometer (ThermoFisher Scientific), pooled and sequenced on an Illumina NovaSeq 6000 instrument using 100 bp single-end reads.

Flow cytometry

Cells were analyzed using a CytoFLEX S flow cytometer (Beckman Coulter) and the resulting data was processed in FlowJo (BD).

Immunoblotting

Cells were washed with PBS and lysed in 1% SDS plus 1:200 Benzoylase (Merck, #E1014) at room temperature for 20 minutes. Following the addition of Laemmli buffer supplemented with β -mercaptoethanol, the lysates were heated at 70°C for 10 minutes and separated by SDS-PAGE. Proteins were transferred onto PVDF membranes (Merck, #IPFL00010) using the Trans-Blot SD Semi-Dry Transfer Cell (Bio-Rad). The membranes were blocked with 5% milk in PBS-T (PBS plus 0.2% Tween-20) and incubated overnight at 4°C with primary antibody in 5% milk. After three washes in PBS-T, membranes were incubated with HRP-conjugated secondary antibodies in 5% milk for 40 minutes at room temperature. Finally, after three additional washes with PBS-T, reactive bands were detected using either Pierce ECL Plus Western Blotting Substrate (ThermoFisher Scientific, #32132X3), SuperSignal West Pico Plus (ThermoFisher Scientific, #34580) or SuperSignal West Dura (ThermoFisher Scientific, #34076) chemiluminescent substrates.

Co-immunoprecipitation

Cells were washed once in PBS and lysed in cell lysis buffer (0.1% IGEPAL, 10 mM HEPES, 1.5 mM MgCl₂, 10 mM KCl plus an EDTA-free protease inhibitor cocktail tablet (Roche)) for 10 min on ice. Nuclear pellets were isolated by centrifugation at 800 $\times g$ for 5 minutes at 4°C and resuspended in nuclear lysis buffer (1% IGEPAL plus 1:200 Benzoylase in TBS). Following removal of insoluble nuclear material by centrifugation (10,000 $\times g$ for 10 minutes at 4°C), nuclear lysates were pre-cleared with protein A or protein G magnetic beads (ThermoFisher Scientific, #88846) for 30 minutes at 4°C on a rotating wheel. Immunoprecipitation was performed by incubating the pre-cleared nuclear lysates with 1 μg of antibody per 10⁷ cells and protein A (for rabbit antibodies) or protein G (for mouse antibodies) magnetic beads for a minimum of 2 h at 4°C on a rotating wheel. The beads were washed five times in lysis buffer and bound proteins eluted by heating at 70°C for 10 min in Laemmli buffer (Bio-Rad, #1610747).

Mass spectrometry analysis

V5-CRAMP1 co-immunoprecipitations were performed as described above, using $\sim 5 \times 10^8$ K562 cells expressing V5-tagged CRAMP1. A V5 pull-down in wild-type cells served as a negative control. Samples were reduced, alkylated and digested using the S-Trap protocol (Protifi, Fairport, NY) with proteins digested overnight using trypsin in 50 mM HEPES pH8. Digested peptides were eluted with sequential washes with 50 mM HEPES and 0.2% formic acid/acetonitrile and pooled in 0.5 ml tubes (Protein LoBind, Eppendorf). Tryptic peptides were dried almost to completion and re-suspended in 20 μl MS solvent (3% MeCN, 0.1% TFA) and 6 μl analysed by LC-MSMS using a Q Exactive Plus coupled to an Ultimate RSLC3000nano UPLC (Thermo Scientific). Peptides were resolved using a 50 cm C18 PepMap EASYSpray column with a gradient rising from 97% solvent A (0.1% formic acid), 10% solvent B (80% acetonitrile, 0.1% formic acid) to 40% solvent B over 45 min. Data were acquired in a data-dependent acquisition fashion with

MS spectra acquired between m/z 400 and 1,500 at 70,000 fwhm. Fragmentation was performed in the top 10 fashion with peptides selected for HCD fragmentation excluded from further fragmentation for 30 s. Raw files were processed in Maxquant 2.2.0.0 with carbamidomethylation (C) as a fixed modification and oxidation (M) and acetylation (protein N-terminus) as variable modifications. Data was searched against a Uniprot Homo sapiens database (downloaded 23/09/20) with LFQ and iBAQ enabled.

Subcellular fractionation

K562 cells were washed with PBS and then in Buffer A (10 mM HEPES (pH 7.9), 1.5 mM MgCl₂, 10 mM KCl, 0.5 mM DTT and an EDTA-free protease inhibitor tablet (Merck, #11873580001)). The cells were then lysed in Buffer A plus 0.1% (v/v) IGEPAL on ice for 10 minutes, and the nuclei were pelleted by centrifugation (1400 $\times g$ for 4 min at 4°C). The supernatant was collected as the cytoplasmic fraction. Nuclei were lysed in Buffer B (20 mM HEPES (pH 7.9), 1.5 mM MgCl₂, 300 mM NaCl, 0.5 mM DTT, 25% (v/v) glycerol, 0.25% Triton X-100, 0.2 mM EDTA and an EDTA-free protease inhibitor tablet (Merck, #11873580001)) on ice for 10 minutes. The insoluble nuclear material (containing chromatin) was pelleted by centrifugation (1700 $\times g$ for 4 min at 4°C), and the supernatant, containing the nucleoplasmic fraction, was collected. The chromatin fraction was solubilized in Laemmli buffer plus β -mercaptoethanol and 1:100 Benzonase (Merck, #E1014).

CRISPR/Cas9-mediated gene disruption

Single guide RNA (sgRNA) sequences were selected from the Sabatini/Lander Human CRISPR Pooled Library (Addgene #1000000100, kindly deposited by David Sabatini and Eric Lander⁸¹) or the Brunello Human CRISPR Knockout Pooled Library (Addgene #73178, kindly deposited by David Root and John Doench⁸²). Oligonucleotides corresponding to top and bottom strands of the sgRNAs (Merck) were phosphorylated with T4 PNK (NEB, #M0201), denatured by heating to 95°C, annealed by cooling to 4°C at a rate of 0.1°C/s and then cloned into the lentiviral sgRNA expression vector pKLV2-U6gRNA(BbsI)-PGKpuro2ABFP-WPRE (Addgene #67974, kindly deposited by Kosuke Yusa⁸⁰). To generate CRAMP1 and SUZ12 knockout clones, cells were first transduced with pHR SIN-pSFFV-Cas9-pPGK-Blasticidin^R, selected with blasticidin and then transduced with the lentiviral sgRNA expression vectors (see Table S11) and selected with puromycin. The resulting populations were single cell cloned using a FACSAria II (BD) cell sorter. Successful gene disruption in the resulting clones was confirmed by immunoblot.

shRNA-mediated knockdown

Short hairpin RNA (shRNA) sequences (see Table S11) were designed using the Broad Institute's Genetic Perturbation Platform (<https://portals.broadinstitute.org/gpp/public/seq/search>). Oligonucleotides corresponding to top and bottom strands (Merck) were phosphorylated with T4 PNK (NEB, #M0201), denatured by heating to 95°C, annealed by cooling to 4°C at a rate of 0.1°C/s and then cloned into the lentiviral shRNA expression vector pHR-SIREN (a kind gift from Prof. Paul Lehner⁸³). Cells were transduced with the target lentiviral shRNA expression vectors and selected with puromycin. Successful shRNA-mediated depletion was confirmed by immunoblot seven days post-transduction.

RT-qPCR

Total RNA was isolated using the RNeasy kit (Qiagen, #74106). Genomic DNA was eliminated by on-column DNase I digestion (Qiagen, #79256). RNA was converted into cDNA using LunaScript RT SuperMix (NEB, #M3010) according to the manufacturer's protocol. Quantification by qPCR was conducted on a StepOne Real-Time PCR System (ThermoFisher Scientific) using Luna Universal qPCR Master Mix (NEB, #M3003) as per the manufacturer's protocol. Primer sequences are detailed in Table S11.

RNA-seq

Total RNA was isolated using the RNeasy kit (Qiagen, #74106). Genomic DNA was eliminated by on-column DNase I digestion (Qiagen, #79256). Ribosomal RNA was depleted with the NEBNext rRNA Depletion Kit v2 (NEB, #E7405). The NEBNext Ultra II Directional RNA Library Prep Kit for Illumina (NEB, #E7760) was used to prepare multiplexed sequencing libraries, which were sequenced on an Illumina NovaSeq 6000 instrument (122 bp single-end reads).

CUT&RUN

CUT&RUN was performed using 5 $\times 10^5$ K562 cells with the CUTANA CUT&RUN kit (EpiCypher, #14-1048) following the manufacturer's instructions. Targets were enriched using 0.05 μ g primary antibody, with the exception of SUZ12 where 0.5 μ g antibody was used. The NEBNext Ultra II DNA Library Prep Kit for Illumina (NEB, #E7645) was used to generate multiplexed sequencing libraries, which were sequenced on an Illumina NovaSeq 6000 instrument (122 bp single-end reads).

CUT&Tag

CUT&Tag was performed using 1 $\times 10^5$ cells with the CUTANA CUT&Tag kit (EpiCypher, #14-1102) following the manufacturer's instructions. Target binding sites were enriched using 0.5 μ g primary antibody, with the exception of knockdown and knockout experiments where 0.05 μ g antibody was used. Multiplexed sequencing libraries were sequenced on an Illumina NovaSeq 6000 instrument (61 bp paired-end reads, with the exception of knockdown experiments where 122 bp single-end reads were used).

ChIP-seq

Wild-type N2 *C. elegans* were grown at 20°C in liquid culture using standard S-basal medium and HB101 *E. coli*.⁸⁴ To isolate embryos, worms were bleached and the eggs hatched for 20–22 h at 25°C in M9 buffer. Starved L3 larvae were grown at 20°C for 30 h, floated on sucrose and flash frozen in liquid nitrogen. ChIP-seq was performed as described in ref McMurchy et al.⁶⁸ Briefly, frozen L3 worms were ground to a powder and fixed with 1.5 mM ethylene glycol bis(succinimidyl succinate) (EGS) (ThermoFisher, #21565) in PBS for 8 minutes, followed by an additional formaldehyde fixation (1% for a further 8 minutes). The reaction was quenched by adding glycine to a final concentration of 0.125 M for 5 min. The fixed tissue was washed twice in PBS containing a protease inhibitor cocktail tablet (Roche, #05056489001) and once in FA buffer (50 mM HEPES pH7.5, 1 mM EDTA, 1% Triton X-100, 0.1% sodium deoxycholate, 150 mM NaCl and protease inhibitors). Following resuspension in FA buffer (1 ml buffer per 1 ml of ground worm powder), the extract was sonicated to an average size of ~250 bp using a Bioruptor Pico (Diagenode). ChIP was performed in duplicate using 20 µg of DNA and 2 µg of HIS-24 antibody. ChIP-seq libraries were prepared according to ref Jänes et al.⁶⁷.

ATAC-seq

ATAC-seq was performed using 50,000 K562 cells with the Diagenode ATAC-seq kit (#C01080001) according to the manufacturer's protocol. Multiplexed sequencing libraries were sequenced on an Illumina NovaSeq 6000 instrument (61 bp paired-end reads).

AlphaFold 3 structural prediction

The AlphaFold 3⁴⁸ server was used to predict interactions between the CRAMP1 (residues E164–D230), FLASH (G1923–R1982) or GON4L (T2149–E2209) SANT domains and the NPAT C-terminus (L1406–E1427), as well as interactions between the CRAMP1 UBL domain (K313–V757) and the GON4L PAH domains (P1621–A1780). Models were visualized in UCSF ChimeraX.⁷⁸

QUANTIFICATION AND STATISTICAL ANALYSIS

CRISPR/Cas9 genetic screen

Raw sequence reads trimmed of sgRNA constant regions using Cutadapt and aligned to a library index using Bowtie 2.⁷⁶ Reads that aligned uniquely to each sgRNA were enumerated and then MAGeCK³⁷ was used to identify genes targeted by sgRNAs that were significantly enriched in the selected cells compared to the unselected library. For the scatterplot shown in Figure 1C, all targeted genes were arranged alphabetically on the x-axis, and “Significance” on the y-axis represents the $-\log_{10}$ of the MAGeCK “pos|score” metric.

RNA-seq

Illumina adaptor sequences were removed using Cutadapt,⁸⁵ and the trimmed reads were then mapped to the human genome (GRCh38) using Bowtie 2.⁷⁶ Uniquely mapped reads with a MAPQ score greater than 20 were imported into SeqMonk (Babraham Bioinformatics Group), where they were analyzed using the RNA-seq quantitation pipeline and DESeq2.⁷⁷ Gene ontology term enrichment analyses were conducted using g:Profiler.⁷⁴

To determine the chromatin landscape across upregulated genes (Figure 6F), the number of histone modification peaks overlapping (+/- 5 kb) genes significantly upregulated upon CRAMP1 or SUZ12 knockdown was quantified with BEDTools⁷⁵ using K562 ChIP-seq data from ENCODE (see CUT&Tag below). Following normalization to account for gene length, fold enrichment was calculated by comparing the mean number of peaks per gene in genes upregulated with shCRAMP1 and shSUZ12 (n=636) versus genes whose expression remained unchanged (n=34,824).

To determine the relative levels of repressive histone modifications found across upregulated genes (Figure 6G), H3K27me3 (ENCF915XIL) and H3K9me3 (ENCF559DHZ) levels were quantified across genes significantly derepressed upon CRAMP1 or SUZ12 knockdown using BEDTools⁷⁵ *multicov*. Read counts were normalized to account for gene length.

CUT&RUN

Reads were aligned to the human genome (GRCh38) using Bowtie 2⁷⁶ (*local, very-sensitive, no-unal, no-mixed, no-discordant, phred33, l 10, X 700*). V5-CRAMP1 peak calling was performed using the MACS2⁸⁶ *callpeak* function relative to V5 control ($P < 1 \times 10^{-10}$) and assigned to the nearest TSS using HOMER.⁷² RPKM-normalized bigwig files were created with deepTools⁷³ *bamCoverage*; heatmaps were generated using *computeMatrix*, *plotHeatmap* and *plotProfile*. Data was visualized in IGV.⁷¹ Peak calling for SUZ12 was performed relative to IgG using the implementation of the MACS peak caller in SeqMonk (window size = 800 bp and $P < 1 \times 10^{-9}$).

CUT&Tag

Reads were aligned to the human genome (GRCh38) using Bowtie 2⁷⁶ (*local, very-sensitive, no-unal, no-mixed, no-discordant, phred33, l 10, X 700*). Peak calling was performed using the implementation of the MACS peak caller in SeqMonk with the following parameters: H3K27me3 relative to IgG (window size = 800 bp and $P < 1 \times 10^{-5}$), and H1 relative to the respective H1 KO clone (window size = 800 bp and $P < 1 \times 10^{-7}$, except for H1.2 where $P < 1 \times 10^{-5}$ was used). H1 peaks (Figure 4) were derived by combining individual

H1 peak lists and intersecting overlapping peaks using BEDTools⁷⁵ *merge*. RPKM-normalized bigwig files were created with deepTools⁷³ *bamCoverage* and visualized in IGV.⁷¹ Heatmaps and profile plots were generated using deepTools⁷³ *computeMatrix*, *plotHeatmap* and *plotProfile*.

Correlations between endogenous and FLAG-tagged H1 subtypes (Figure S4B) were performed using deepTools⁷³ *multiBamSummary* (binSize = 5,000) and *plotCorrelation* (Spearman). Pairwise correlations between individual endogenous and FLAG-tagged H1 subtypes (Figure S4E) were conducted using deepTools⁷³ *multiBamSummary* (binSize = 5,000, outRawCounts option). To plot the pairwise correlations, raw counts were log-transformed after adding 1 to all to avoid zero values, and a linear regression was fitted to calculate the R² values.

To calculate the enrichment of H1 CUT&Tag signal over genomic regions marked by particular histone modifications in various human cell lines (Figures 4B and S5B), BEDTools⁷⁵ *multicov* was used to count the number of H1 reads over each histone modification peak. Read counts were then normalized to the total read count, divided by the respective IgG or FLAG control, and log-transformed to calculate the final enrichment. For K562 cells, the following ChIP-seq datasets were downloaded from ENCODE⁵³: H3K4me1 (ENCFF839DZV), H3K4me2 (ENCFF446FUS), H3K4me3 (ENCFF633WWH), H3K9ac (ENCFF149MXA), H3K9me3 (ENCFF744MLH), ENCFF928ZQM), H3K27ac (ENCFF232RQF), H3K27me3 (ENCFF915XIL, ENCFF330YFF), H3K36me3 (ENCFF925FDY), H3K79me2 (ENCFF711PLM) and inputs (ENCFF355SGP was used to call H3K27me3 peaks and ENCFF893MMO was used to call all other peaks). All bam files downloaded from ENCODE were pre-processed using standard ENCODE pipelines and were visually assessed using IGV⁷¹ to ensure data quality. Peak calling was performed using the implementation of the MACS peak caller in SeqMonk (window size = 300 bp and $P < 1 \times 10^{-5}$, except for H3K4me3 where $P < 1 \times 10^{-8}$ was used). For HCT116 cells, the following ChIP-seq datasets were downloaded from ENCODE⁵³: H3K4me1 (ENCFF485QHQ), H3K4me2 (ENCFF205HPZ), H3K4me3 (ENCFF178EXO), H3K9ac (ENCFF676ASZ), H3K9me3 (ENCFF568HSD), H3K27ac (ENCFF087TXX), H3K27me3 (ENCFF271HVJ), H3K36me3 (ENCFF412ONB), H3K79me2 (ENCFF949CYK), H4K20me1 (ENCFF085FNO) and input (ENCFF373OZW). Peak calling was performed using the implementation of the MACS peak caller in SeqMonk (window size = 300 bp and $P < 1 \times 10^{-5}$, except for H3K9me3, H3K27me3 and H4K20me1 where window size = 600 bp and $P < 1 \times 10^{-5}$, and H3K27ac where window size = 300 bp and $P < 1 \times 10^{-6}$). For RPE-1 cells, the following histone modification peaks were used: H3K4me3 (GEO, GSM4194686), H3K9me3 (ChIP Atlas, DRX002909) and H3K27ac (GEO, GSM4194692). H3K27me3 peaks were called from CUT&Tag data with MACS2⁸⁶ (broad mode, broad-cutoff = 1). For Jurkat cells, ChIP-seq peaks were obtained from ENCODE (H3K4me3, ENCFF305JOT) or GEO (H3K9me3, GSE162605 and H3K27ac, GSE115438). H3K27me3 peaks were called from CUT&Tag data with MACS2⁸⁶ (broad mode, broad-cutoff = 0.1). H1 and H3K27me3 CUT&Tag data from murine CD8⁺ T cells generated by the Skoultchi laboratory (Figure S5D) was downloaded from GEO (GSE153543)²⁴ and converted to bigwig files using UCSCtools⁸⁷ *bedGraphToBigWig*. Data was visualized using IGV.⁷¹

ChIP-seq

The following ChIP-seq datasets were downloaded from GEO: H3K27me3 (GSM3141784, GSM3141785), H3K4me3 (GSM3141748), H3K36me3 (GSM3141772) and input (GSM2333112 and GSM2333111). Reads were aligned to the *C. elegans* genome (ce11) using Bowtie 2⁷⁶ (*local, very-sensitive, no-unal, no-mixed, no-discordant, phred33*). RPKM-normalized bigwig files were created with deepTools⁷³ *bamCoverage* (extending reads by 200 bp) and visualized in IGV.⁷¹ H3K27me3 peaks were called using MACS2⁸⁶ (broad mode, broad-cutoff = 0.05) and profile plots were created using deepTools⁷³ *computeMatrix* and *plotProfile*. Datasets were correlated using deepTools⁷³ *multiBamSummary* (binSize = 1,000 bp) and *plotCorrelation* (Spearman). The additional H1 ChIP-seq datasets used in this study were mouse H1.4 (GEO, GSM5770168),⁴⁹ mouse H1.0 (GEO, GSE215266)¹⁰ and human H1.2 and H1.5 (GEO, GSE136264).¹⁷ Reads were mapped to the mouse (mm10) or human (GRCh38) genomes, respectively, using Bowtie 2⁷⁶ (*very-sensitive, local, no-mixed, no-discordant, dovetail, phred33, I 10, X 700*). RPKM-normalized bigwig files were created with deepTools⁷³ *bamCoverage* and visualized using IGV.⁷¹

ATAC-seq

Raw fastq files were processed using the nf-core atacseq v2.1.2 pipeline executed using nextflow v24.01.0. Low-confidence peaks were filtered out (fold-change < 3.5 in both replicates), and the change in accessibility across the remaining high-confidence peaks was assessed using DESeq2.⁷⁷ RPKM-normalized bigwig files were generated by the nf-core atacseq pipeline and accessibility changes were visualized using IGV⁷¹ and deepTools⁷³ *computeMatrix*, *plotHeatmap* and *plotProfile*. Peaks displaying differential accessibility were assigned to promoters using HOMER⁷² and to enhancers with BEDTools⁷⁵ *intersect* (using annotated enhancers in K562 cells (ENCFF815ILK)^{53,88}). Enrichment analysis of GO terms was conducted using g:Profiler.⁷⁴

To quantify the changes in accessibility across genomic regions marked by particular histone modifications (Figure 7D), normalized ATAC-seq read counts were quantified across histone modification peaks in K562 cells (see CUT&Tag above) using BEDTools⁷⁵ *multicov*. Low-confidence regions (total read count across all conditions < 150) were removed, and the remaining read counts were used to calculate the fold-change in accessibility across each peak relative to the shControl sample. The median values for each histone modification were plotted.